The cytotoxic effect and molecular targets of ezetimibe in A549 lung cancer cells

by

CHAMONÉ MUNNIK (63280086)

submitted per the requirements for the degree of

MAGISTER SCIENTIAE

in the subject

BIOCHEMISTRY

at the

UNIVERSITY OF SOUTH AFRICA

SUPERVISOR: PROFESSOR M. NTWASA

CO-SUPERVISOR: DR. S.A. SOOKLAL

2023

Abstract

The p53 gene is a well-known tumour suppressor gene, shown to be dysfunctional in more than 50% of human malignancies. The cellular significance of this oncogene is evident in a series of diverse cellular antiproliferation properties owing to specified cell-cycle checkpoint arrest, cellular senescence, and apoptosis. The multifunctionality of p53 indicates the importance of this protein while also hinting at the diverse regulatory mechanisms required for function and regulation. Since most tumours display dysfunction of p53, considerable efforts are made in the development of cancer therapies exploiting the functions and mutations of p53. MDM2 is a known primary negative regulator of p53. The tight control exhibited by MDM2 on p53 suggests that inhibiting MDM2 could translate to anti-cancerous effects. *In silico* methods identified ezetimibe (brand-named Zetia) as a potential anti-cancer drug. The computational model revealed high-affinity binding between ezetimibe and the MDM2 hydrophobic cleft of the MDM2 p53-binding site. The observed structure indicates inhibition of p53 binding when MDM2 is bound to ezetimibe, thus preventing the formation of MDM2-p53 complexes. The reduced downregulation of p53 could have immense oncological potential. This study aims to investigate the cytotoxic effect of ezetimibe on A549 lung cancer cells for its potential use as an anti-cancer agent. The safety and efficacy of the drug were monitored on mammalian cells by MTT assay. The analysis of molecular underpinnings of cellular changes caused by ezetimibe was determined with the use of Flow Cytometry, to characterise apoptosis and cell cycle analysis. Moreover, molecular targets of ezetimibe were evaluated using the Drug Affinity Responsive Target Stability (DARTS) method. It should be noted that this study did not investigate the molecular underpinnings of the identified molecular targets. The integrated investigation of the molecular targets is assigned for future studies. This study, therefore, aimed to validate the use of ezetimibe as a viable cancer treatment. The results revealed that ezetimibe is toxic to the A549 cells and not toxic to normal cells and MCF-7 cells at the same concentrations. The cellular changes caused by ezetimibe in apoptosis and cell cycle analysis were consistent with p53 activity. While ezetimibe induced cellular changes in A549 cells, the effect was limited. Finally, the molecular targets of ezetimibe provided numerous proteins with potential therapeutic capacity. While the identified proteins revealed an agglomeration of functions, future pathway analysis is required. This study demonstrated the efficacy of ezetimibe as an anti-cancer agent for A549 human lung cancer cells.

Declaration

I, Chamoné Munnik, am a registered student at the University of South Africa (UNISA) in the academic year of 2022, for the degree of Master of Science (MSc). In the submission of this MSc dissertation, I hereby declare that "**The cytotoxic effect and molecular targets of ezetimibe in A549 lung cancer cells**" is my work.

I am aware of plagiarism and testify that all sources have been indicated and acknowledged. I understand that the University of South Africa (UNISA) has the right to take disciplinary action against me if plagiarism is suspected. I also declare that this dissertation has not been submitted before, at this or any other University, for another degree or examination.

Chamoné Munnik

Date: 30 January 2023

Acknowledgements

The grace of God has brought me to this moment. The way He has directed my path and education is better than any way I could have envisioned for myself. I trust in Him still and pray for the courage to follow His plan for my future. Every highlight and every low point I give to Him. Knowing, that without God, none of my accomplishments would have been possible.

To Professor Monde Ntwasa, my supervisor on this project, I want to thank you for the guidance you provided. The kindness and the insight I have received from Prof. was a rare and wonderful combination, without which I would not have reached this point in my studies.

Dr Selisha Sooklal, my co-supervisor, you deserve more praise than I could convey. Thank you for always going over and beyond for me. You have inspired me academically and personally with your invaluable work ethic and kind and respectful approach to life.

Mr Sibusiso Malindisa, for always finding the time to help and always doing so with a smile.

Dr Bonnie Russell for your thoughtful help and encouragement.

Lerato for your helpful assistance on the BD FACSAria™ II cytometer.

My fellow master's students, you have helped me so much on this journey.

The Fly Lab members for being such a great team. I am proud to say I was a part of it.

UNISA for their financial assistance.

To my family and friends for your steadfast patience and support. You mean the world to me.

To my husband, you have been my greatest supporter and cheerleader. You encouraged me to pursue my passion and strengthened me every step of the way. You kept my spirit light, and my mind determined. I am grateful for your dedication to my academic pursuits, knowing how much they mean to me. You are my true delight.

Research Output

Publications:

Review Article:

Munnik, C., Xaba, M.P., Malindisa, S.T., Russell, B.L., & Sooklal, S.A. 2022. *Drosophila melanogaster*: A platform for anticancer drug discovery and personalized therapies. *Frontiers in genetics*, 13:949241. https://doi.org/10.3389/fgene.2022.949241

Table of Contents

List of Abbreviations

3T3DM: Transformed Balb/c 3T3 cell line
A549: Human epithelial lung carcinoma cell line
AKT: Protein kinase B
APS: Ammonium Persulfate
ATM: Ataxia-telangiectasia mutated
ATR: Rad3-related protein
BAX: Bcl-2 associated X protein
Bcl-2: B-cell lymphoma-2
c-Abl: Tyrosine kinase
Cdc2: Cyclin-dependent kinase 1 (cyclin E and cyclin A)
Cdk2: Cyclin-dependent kinase 1 (cyclin B and cyclin A)
cdk2: Cell division stimulating protein 2
Chk1: Checkpoint kinase 1
Chk2: Checkpoint kinase 2
CI: Cell Index
CK1: Casein kinase 1
CK2: Casein kinase 2
DARTS: Drug affinity responsive target stability
DMEM: Dulbecco's Modified Eagle Medium
DMSO: Dimethyl sulfoxide
DNA: Deoxyribonucleic acid
DNA-PK: DNA-dependent protein kinase
DSB: Double-strand breaks
DWNN: Domain with no name
ER: Endoplasmic reticulum
FBS: Fetal bovine serum
GADD45: Growth arrest and DNA damage-inducible protein 45
GSK3: Glycogen synthase kinase 3
HEK293: Immortalized human embryonic kidney cell line
IC_{50}: Half-maximal inhibitory concentration
JNK: c-Jun N-terminal kinase
LC: Liquid chromatography
LC-MS: Liquid chromatography-mass spectrometry

LDL-C: Low-density lipoprotein cholesterol
MCF-7: Human breast cancer cell line
MDM2: Murine double minute 2
MDMX: Homologue of MDM2
mRNA: Messenger ribonucleic acid
MS: Mass spectrometry
MW: Molecular weight
NES: Nuclear export sequence
NLS: Nuclear localization sequence
NOXA: Phorbol-12-myristate-13-acetate-induced protein 1
NPC1L1: Niemann-Pick C1-like 1
NSCLC: Non-small cell lung carcinoma
P2P-R: Proliferation potential protein-related
PACT: Protein kinase, interferon-inducible double-stranded RNA-dependent activator
PBS: Phosphate-buffered saline
PI: Propidium iodide
PIKKs: PI3K-related serine/threonine kinases
pRb: Retinoblastoma protein
PRD: Proline-rich domain
PS: Phosphatidylserine
PUMA: p53 upregulated modulator of apoptosis
Ras: Small GTPase protein
RBBP6: Retinoblastoma binding protein 6
REG: C-terminal regulatory region
RING: Really Interesting New Gene
RP: Regulatory particle
RQ1: Homologue of RBBP6
ssDNA:Single-stranded DNA
SCLC: Small cell lung carcinoma
SD: Standard deviation
SDS: Sodium dodecyl-sulfate
SDS-PAGE: Sodium dodecyl-sulfate polyacrylamide gel electrophoresis
TAFII250: Transcriptional initiation factor TFIID subunit 1
TAD: Transcriptional activation domain
TEMED: Tetramethylethylenediamine
TET: Tetramerization domain
Zn: Zinc finger region

List of Figures

List of Tables

Chapter 1: Literature Review

1.1 Introduction

In humans, the formation of malignant tumours requires progressive genetic alterations, these alterations include the activation of dominant oncogenes as well as the deactivation of tumour suppressor genes (Homer *et al*., 2005; Roth *et al*., 1998). The oncological significance of the tumour suppressor gene *TP53* is evident in that more than half of human cancer types reported inactivity of *TP53* (Hollstein *et al*., 1991; Vogelstein and Kinzler, 1992). This p53 protein safeguards genomic integrity through the process of cell-cycle arrest, repairing of DNA, cellular senescence, and apoptosis (Beckerman & Prives, 2010; Zilfou & Lowe, 2009). The mutation of p53 is highly variable based on the type of cancer.

The regulation of p53 is predominantly controlled by murine double minute 2 (MDM2). Acting as an oncoprotein, MDM2 is the chief negative regulator of p53 governing the activation and stabilization of this tumour suppressor. MDM2 modulates the MDM2-p53 signalling pathway through post-translational modifications, managing cellular p53 activity (Chen *et al*., 1993; Oliner *et al*., 1993). These functions of MDM2 are significant in normal cells, however, in cancer cells MDM2 suppresses p53 and the vital functions of p53 are neglected. MDM2 is known as a p53-responsive gene, meaning that *MDM2* transcription is activated by increased levels of p53. Elevated MDM2 levels have been noted in many cancer types (Carr & Jones, 2016; Cordon-Cardo *et al*., 1994; Leach *et al*., 1993; Oliner *et al*., 1992). Theoretically, the prevention of p53 degradation would lead to the induced apoptosis of cancer cells. Potential therapeutic responses may be presented by targeting this MDM2-p53 interaction.

Ezetimibe is a potential anti-cancer drug, investigated for its ability to modulate MDM2 concentration levels. The ezetimibe-MDM2 complex formation is illustrated in a docking experiment utilizing drug databases to identify prospective target molecules for p53-regulated cancer treatments (Twala, 2017). Ezetimibe was identified as interacting with the N-terminal p53-binding region of MDM2 through an array of ligands forming a stereochemical connection with MDM2 residues (Twala, 2017). The initial association of ezetimibe to MDM2 causes a cascade of binding activities culminating in the tightly bound ezetimibe-MDM2 complex (Twala, 2017). By controlling the regulators of p53, control is governed over p53 itself and potentially tumorigenesis.

1.2 Lung cancer

1.2.1 The statistical data and current therapies for lung cancer

Lung cancer has the highest statistical mortality rate among cancer types, claiming 1.8 million lives in 2020 (Sung *et al*., 2021). Histologically, lung cancer tumours are broadly categorised as non-small cell lung carcinomas (NSCLC) and small cell lung carcinomas (SCLC). Statistically, approximately 85% of lung cancers are recorded as NSCLC, 40% as adenocarcinomas, 25% as squamous cell carcinomas, and 10% as large cell carcinomas (Chansky *et al*., 2017). SCLC has been shown to progress rapidly with a high probability to metastasise, leading to extensive-stage small-cell lung cancer in 80-85% of patients upon diagnosis (Mar *et al*., 2019). While NSCLC is less likely to metastasise, this cancer is reportedly less sensitive to chemotherapy or radiation treatment compared to SCLC.

The high mortality rate associated with this cancer alludes to the lack of effective and sustainable treatment options available. The conventional treatment for lung cancer consists of chemotherapy, radiation and surgically removing the tumour cells. These treatments induce adverse side effects and are often unsuccessful. Technological advances have allowed for personalized treatment plans based on drugs that block cancer related genetic pathways (Herbst *et al*., 2018). This form of oncological treatment proves more effective and allows for better quality of life compared to conventional therapies (Politi & Herbst, 2015).

1.2.2 TP53 mutations in lung cancer

Approximately 50% of NSCLC report a mutation in the TP53 gene, marking this gene as oncological significant in the treatment of lung cancer (Bodner *et al*., 1992). Additionally, SCLC reported the highest number of TP53 mutations. These mutations to TP53 occur early in lung cancer development and are maintained throughout tumor progression and metastasis (Harris, 1996; Sozzi et al., 1995). The phenotypical alterations to TP53 prevents the correct expression of this gene, and consequently affects numerous cytological processes. The prevalence of TP53 mutations in lung cancer promotes the study and exploitation of TP53 and associated pathways to improve lung cancer mortality rates.

1.3 The p53 protein

1.3.1 The structure of p53

The p53 protein is also known as the tumour protein 53, with this name originating from the molecular mass (53kDa) during its simultaneous discovery by numerous independent scientists (DeLeo *et al*., 1979; Kress *et al*., 1979; Lane & Crawford, 1979; Linzer & Levine, 1979). The technique of SDS-PAGE was used in establishing the size of the protein, with this specification later linking the research. It is to be noted that an amino acid residue calculation reveals the protein's mass to be 43.7kDa.

The p53 protein is encoded by the *TP53* gene. Situated on the short arm of chromosome 17, this gene was only characterised as a tumour suppressor gene in 1989, a decade after its initial discovery (Baker *et al*., 1989; Finlay *et al*., 1989). A study by Baker and co-workers (1989) investigated both the presence and oncological importance of the *TP53* gene based on the deletion of chromosomal bands 17p12 to 17p13.3. The high percentage of carcinoma activity associated with the allelic deletion of the localised 17p region initiated the investigation. The high cancer probability affiliated with the absence of the *TP53* gene validates the title of "the guardian of the genome" as given to the protein.

1.3.2 The expression of p53

In the event of cellular stress manifesting as DNA damage, oncogenesis, cellular hypoxia, or contact inhibition, p53 gene expression is initiated (Feng & Levine, 2010; Vousden & Prives, 2009). Activation signals rapidly elevate p53 levels principally through protein stabilization and the actuation of p53 DNA binding abilities as controlled by the phosphorylation of the protein. The increased concentration of p53 in turn prevents cells from entering the S phase of the cell cycle through G0/G1 progression inhibition, allowing for the repair of DNA before replication (Bates & Vousden, 1996; Mercer *et al*., 1990). Checkpoint activation requires DNA damage recognition.

Cellular response to DNA damage is predominantly controlled by ataxia-telangiectasia mutated (ATM) and Rad3-related protein (ATR). ATM is activated by DNA damage agents causing DNA double-strand breaks (DSB), while recruitment to single-stranded DNA (ssDNA)

regions in turn activates ATR. The affiliated DNA-dependent protein kinase (DNA-PK) is the primary regulator of a small subclass of proteins integral to DSB end joining. Recognition of DNA damage by numerous sensor proteins enables specialised kinases proteins to trigger the phosphorylation of various effector proteins either directly or indirectly promoting cell-cycle arrest, DNA repair procedures and apoptosis using signalling networks (Ciccia & Elledge, 2010; Jackson & Bartek, 2009) (Figure 1.1). Serine/threonine kinases, ATM and ATR participate in the early-stage identification of cellular damage. Collectively known as PI3K-related serine/threonine kinases (PIKKs), ATM and ATR phosphorylate the Ser15 residue on p53, with more than 10 subsequent kinases also reportedly involved in p53 phosphorylation (Banin *et al*., 1998; Canman *et al*., 1998; Siliciano *et al*., 1997). Lack of functional ATM kinase is exhibited in A-T cells derived from ataxia-telangiectasia patients prone to cancer, leading to radiosensitivity and chromosomal instability. These cells demonstrate a delayed response of p53 upregulation activated by ionising radiations correlating to a delay in phosphorylation of Ser15 residues within the amino-terminal transactivation domain of *TP53* (Siliciano *et al*., 1997).

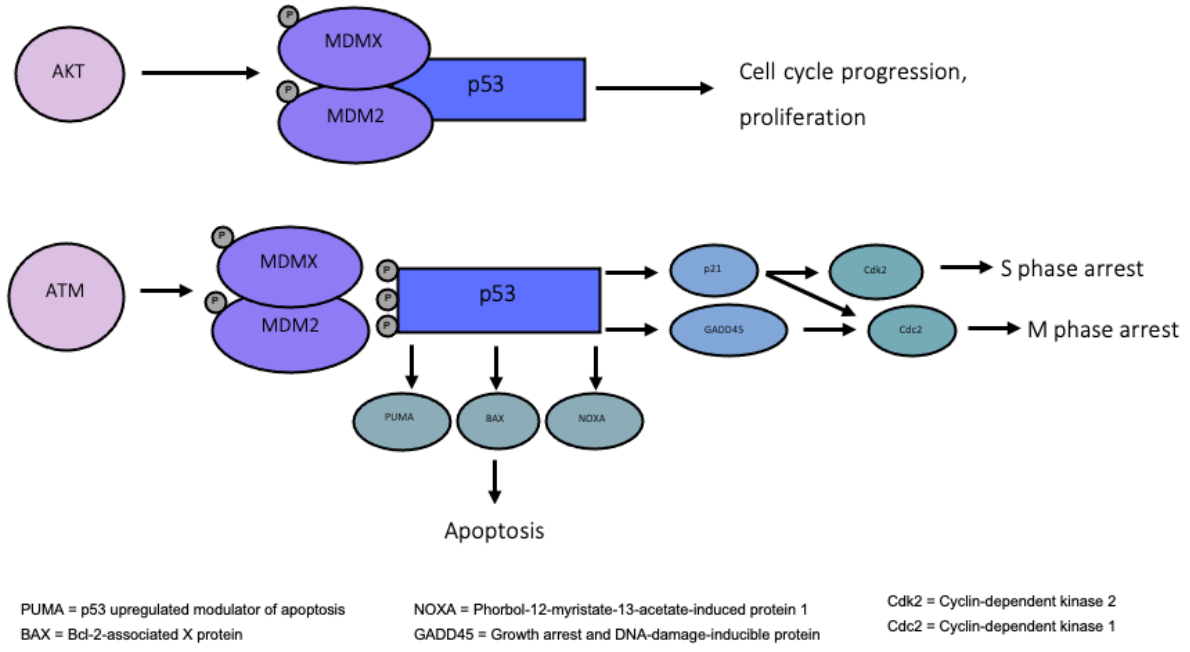

Figure 1. 1: **p53 pathways leading cell cycle progression, cell cycle arrest or apoptosis.** The signalling pathway of p53 in response to DNA damage is shown, as mediated by MDM2. Initiated by permissive growth conditions, the phosphorylation of MDM2 and MDMX stabilises and activates p53. Elevated p53 levels activate downstream genes associated with cell cycle arrest (p21 and GADD45 via protein kinases Cdk2 and Cdc2) and apoptosis (PUMA, BAX and NOXA).

The phosphorylation of p53 occurs on a cluster of residues primarily located at the N- and C-terminal regions (Meek, 2015; Meek & Anderson, 2009) (Figure 1.2). Phosphorylation of the N-terminal amino acid residues is shown to regulate the MDM2-p53 interaction, whereas C-terminal phosphorylation influences the site-specific binding of p53 (Meek, 2015). In response to cellular exposure to IR and UV light, residues Ser6, Ser9, Ser15, Ser20, Ser33, Ser37, Ser46, Thr18, and Thr81 appear to facilitate the phosphorylation of the N-terminal domain of p53 (Meek & Anderson, 2009). The phosphorylation of p53 is primarily controlled by ATM, ATR, and DNA-PK (Banin *et al*., 1998; Canman *et al*., 1998; Lees-Miller *et al*., 1992). Additionally, the ATR- and ATM-activated checkpoint kinases Chk1 or Chk2 also indirectly affect p53 phosphorylation (Saito *et al*., 2002; Shieh *et al*., 2000). Casein kinase 1 (CK1) is another protein indicated in the phosphorylation of p53 through serine and threonine-regulating residues (Dumaz *et al*., 1999; Higashimoto *et al*., 2000).

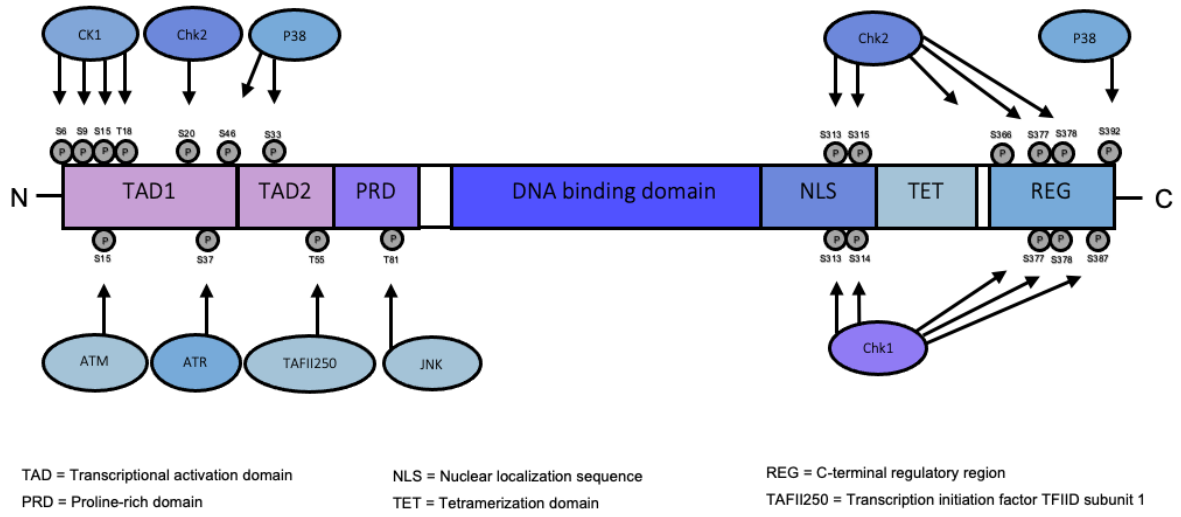

Figure 1. 2: **Domain representation and phosphorylation sites of p53**. The primary functional regions of p53 are shown from the N-terminal to the C-terminal region. The associated kinases known to phosphorylate the p53 protein are identifiable per domain, with the phosphorylation sites indicated by the grey circles entitled P. The specific residue targeted for phosphorylation is shown below the protein kinase.

The phosphorylation of residues Ser15, acts as a target for both ATM and ATR, inhibiting MDM2-p53 interaction and thus the activation of p53 (Shieh *et al*., 1997; Siliciano *et al*., 1997). The phosphorylation of Ser20 mediated by Chk2 also influences p53 concentration by causing the reduction of MDM2-mediated degradation of p53 and coincides with increased activity of p53 (Chehab *et al*., 1999; Hirao *et al*., 2000; Unger *et al*., 1999). Similarly, Thr18 phosphorylation disrupts the binding of MDM2-p53, as intermediated by CK1. The regulation

of p53 by Thr18 is co-dependent on the preliminary phosphorylation of Ser15 (Dumaz *et al*., 1999; Sakaguchi *et al*., 2000). The immediate location of these p53 residues instituted the hypothesis that solely by the phosphorylation of these residues, p53 activation and stabilisation will follow in the event of DNA damage (Kussie *et al*., 1996). Investigation of numerous genetically altered mouse models reveals, however, an insufficient effect on the activation and stabilisation of p53 interceded by DNA damage by the phosphorylating events, as studied under endogenous conditions (Chao *et al*., 2003; Sluss *et al*., 2004).

1.3.3 The function of p53

Upon activation by various protein kinases, p53 functions as a transcriptional regulator facilitating and controlling a magnitude of processes. The multi-functionality of p53 includes the regulatory activity of cell cycle checkpoints (Vousden & Lu, 2002). p53 acts as a precursor in the process of cell cycle arrest by binding DNA and initiating the production of p21. The ability to upregulate p21 expression has a considerable influence on the growth arrest function of p53. The p21 protein sequentially interacts with cell division stimulating protein 2 (cdk2) forming a cdk2-p21 complex. This complex then in turn inhibits the S phase of cellular division. Studies show elevated p21 protein concentration levels in response to DNA damage (Brugarolas *et al*., 1995; Deng *et al*., 1995). In tumour cells lacking a functional p53, Polyak and colleagues (1996) induced the expression of p53, showing the failure to activate cell cycle arrest when the p21 gene is disrupted.

The process of cellular senescence is another well-documented function of p53. A tumorigenesis stimulus is a known trigger for this system characteristic of mitogenic signals, oncogenes, short telomeres and the hyperexpression of some tumour suppressor genes (Itahana *et al*., 2001). Distinct limitations and clearance of tumour development are evident in an *invivo*-induced p53-dependent study observing cellular senescence (Chen *et al*., 2005; Ventura *et al*., 2007; Xue *et al*., 2011). The influence of p53 in the upregulation of p21 is attributed to the senescence-activating qualities of the protein. Increased p21 levels in normal fibroblasts indicate preliminary cellular senescence (Noda *et al*., 1994). The expression of p21 in tumour cells deficient in functional p53 nonetheless promoted cellular senescence (Fang *et al*., 1999; Wang *et al*., 1999).

The inducement of apoptosis appears as a separate function of p53. In a study of transgenic p53-deficient mice, apoptosis activity was induced through gamma radiation in thymocytes, which are for the most part noncycling cells in the G0/G1 phase (Clarke *et al*., 1993; Lowe *et*

al., 1993). Similarly, p53 functionality was rehabilitated in p53 deficient tumour cell lines resulting in cell cycle arrest and apoptosis. The genetic induction of high levels of the apoptosis-blocking Bcl-2 protein impaired the p53-induced apoptosis activity without impeding p53-induced G1/S phase cell cycle arrest (Ryan *et al*., 1994; Selvakumaran *et al*., 1994; Wang *et al*., 1993).

The p53 protein is degraded following the repair of damaged DNA. This degradation by 26S proteasome is targeted by the covalent conjugation of ubiquitin to the protein (Kravtsova-Ivantsiv & Ciechanover, 2012). The 26S proteasome is formed by the 20S core and 19S regulatory particle (RP) protein complexes with protein degradation confined to the central cavity of the 20S core (Bedford *et al*., 2010; Bousquet-Dubouch *et al*., 2011; Gallastegui & Groll, 2010). The 19S RP assists in ubiquitinated protein recruitment, protein unfolding, translocation and deubiquitylation as well as mediating the 20S core entry (Gallastegui & Groll, 2010). The inability to repair damaged DNA places the cell cycle on permanent arrest or the process of apoptosis is initiated. The apoptosis activity, as initiated by p53, follows a tightly controlled transcription-dependent and -independent mechanism promoting efficient cell death as activated by various quantitative and qualitative environmental stimuli (Fridman & Lowe, 2003). In the event of low p53 levels or the inactivity of the protein, damaged DNA is left unaffected to continue into the S phase. The cell cycle progresses to the production of damaged DNA, leading to the formation of neoplastic transformation and in turn genomic instability. The inactivation of p53 is mainly due to mutations or the loss of heterozygous and homozygous alleles. This inactivity of p53 is associated with most cancers (Hollstein *et al*., 1991; Vogelstein and Kinzler, 1992).

1.4 MDM2

The stabilization and activity of p53 are for the most part controlled through the negative regulatory activity of the oncogenic MDM2 protein. The *MDM2* gene was initially isolated from the 50-fold amplified chromosome locus in a murine tumorigenic 3T3DM mouse cell line. This gene has been shown to induce tumorigenesis activity in conjunction with elevated cell expression (Fakharzadeh *et al*., 1991). The tumorigenicity of MDM2 is evident in the overexpression of the protein in soft tissue sarcomas (Cordon-Cardo *et al*., 1994; Oliner *et al*., 1992; Leach *et al*., 1993). The amplification of MDM2 has similarly been identified in various other tumour types, including myeloid neoplasms, B-cell lymphomas, glioblastomas and astrocytomas, breast carcinomas and oral carcinomas (Carr & Jones, 2016).

1.4.1 The structure of MDM2

The amino acid composition of MDM2 identifies a Really Interesting New Gene (RING) finger domain signifying the tumorigenic potential of this protein by influencing cellular growth control mechanisms (Fang *et al*., 2000; Honda & Yasuda, 1999; Kibbutat *et al*., 1997) (Figure 1.3). The MDM2 protein also functions as an E3 ubiquitin ligase of p53, promoting proteasomal degradation and inhibiting p53 transactivity (Haupt *et al*., 1996; Kubbutat *et al*., 1997; Momand *et al*., 1992; Oliner *et al*., 1993). The E3 activity of MDM2 is dependent on the RING finger domain of the protein, located in the C-terminal region (Fang *et al*., 2000). The p53-binding domain allows MDM2 to bind p53, forming an MDM2-p53 conformation-based complex marking p53 for degradation through ubiquitination (Honda *et al*., 1997; Kubbutat *et al*., 1997; Moll & Petrenko, 2003). Reduced levels of MDM2 are thought to promote the monoubiquitylation and nuclear export of p53, while high concentrations of MDM2 induce polyubiquitination and nuclear degradation of the target protein (Gu *et al*., 2001; Li *et al*., 2003). The principle MDM2-ubiquitin ligation site on p53 is located at the C-terminal of the protein with a series of lysine residues targeted by acetylation (Ito *et al*., 2001; Li *et al*., 2002; Nakamura *et al*., 2000; Rodriguez *et al*., 2000). The translocation of MDM2 from the cytoplasm to the nucleus is another mechanism modulating p53 levels, as this leads to an increase in p53 degradation, as facilitated by protein kinase B known as AKT (Gama *et al*., 2009; Mayo & Donner, 2001; Ogawara *et al*., 2002; Zhou *et al*., 2001) (Figure 1.1). AKT reduces p53 protein levels by enhancing the ubiquitination-promoting function of MDM2 through p53 Ser186 phosphorylation (Ogawara *et al*., 2002). The acidic domain of MDM2 influences both MDM2 and p53 degradation. This mechanism is independent of the E3 ligase activity of MDM2 or the cytoplasmic-nuclear translocation facilitating p53 regulation (Argentini *et al*., 2001).

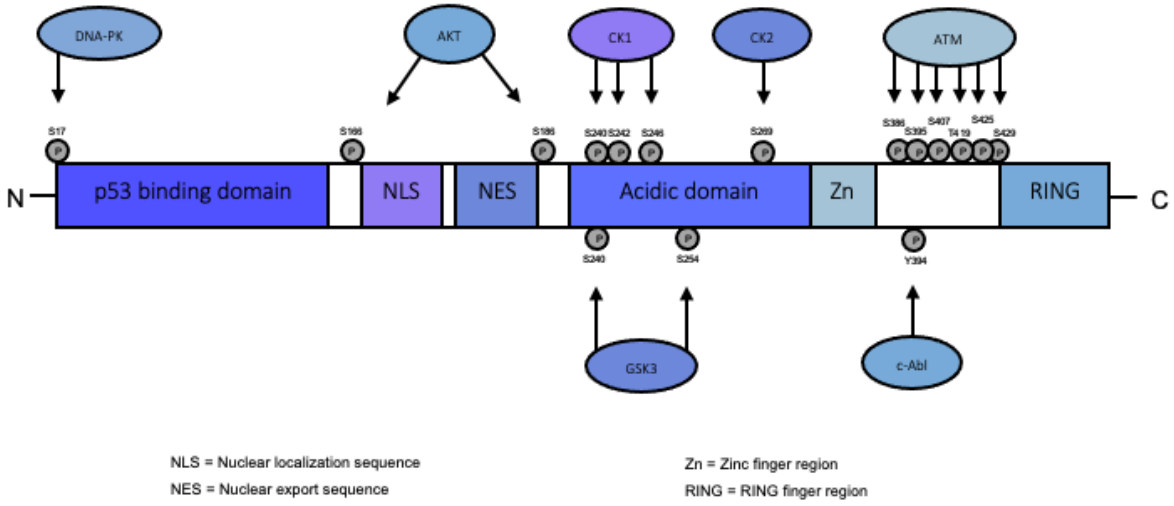

Figure 1. 3: **Domain representation and phosphorylation sites of MDM2**. The primary functional regions of MDM2 are shown from the N-terminal to the C-terminal region. The associated kinases known for the phosphorylation of the MDM2 protein are identifiable per domain, with the phosphorylation sites indicated by the grey circles entitled P. The specific residue targeted for phosphorylation is shown below the protein kinase.

1.4.2 The function of MDM2

The vital functions of p53 are tightly controlled to allow for appropriate differential responses to various stress signals. Stabilization of the p53 gene is dependent on the negative regulatory activity of the MDM2 protein. MDM2 interacts with p53 by binding and simultaneously inhibiting the transactivation domain of p53, thus controlling p53 concentrations (Chen *et al*., 1993; Oliner *et al*., 1993). Correspondingly, the overexpression of MDM2 produces an MDM2-Ras interaction, prompting the transformation of primary cells and inhibiting p53-dependent G1 cell-cycle arrest and apoptosis as indicated in numerous cell lines (Chen *et al*., 1994; Chen *et al*., 1996; Haupt *et al*., 1996).

In the event of cell damage, the p53 protein is phosphorylated, as a process of post-translational modification, preventing the binding of MDM2, which increases p53 levels (de Toledo *et al*., 2000). Phosphorylation is primarily mediated by upstream ATM (serine/threonine molecules) on Ser15, causing a decrease in MDM2 stability (Shieh *et al*., 1997). ATM influences the genome stability, cell-cycle development and damaged DNA responses via the phosphoinositide 3-kinase domain located at the carboxyl domain of the enzyme (Kastan & Lim, 2000; Shiloh, 2001). MDM2 also indicates the capability to direct self-degradation via the

C-terminal RING finger domain (Fang *et al*., 2000; Honda *et al*., 2000). The intensity and duration of a p53-mediated cellular response as a result of an innocuous stress signal demonstrates the molecular complexity of this autoregulated link between MDM2 and p53 expression (Haupt *et al*., 1997; Kubbutat *et al*., 1997; Wu & Levine, 1997). As p53 stabilises and becomes active, it allows for the increased expression of the protein's negative regulator, MDM2. This process maintains an autoregulatory negative feedback loop capable of mediating p53 activity to basal levels.

1.5 Regulation of p53

1.5.1 The activity of p53

The activity of p53 was once believed as non-essential for normal cell growth and differentiation; and only embryonic development may be influenced by the absence of *TP53* (Choi & Donehower, 1999). The low levels of p53 maintained in normal cells due to the rapid degradation of the protein following synthesis implies minimal functionality of p53 in healthy cells (Kibbutat & Vousden, 1998). The efficiency of p53 during tumour development and prevention, however, is essential and this activity requires tight control to ensure the return of normal cellular growth. The role of p53 in normal cells is evident in cellular proliferation and in preventing tumours. Any variations of this control result in profound effects on cell survival (Motoyama *et al*., 2004; Oren, 2003; Sherr & McCormich, 2002). Cellular response during cell cycle arrest and apoptosis include the activation of numerous genes required for impelling cell growth.

1.5.2 MDM2-p53 complex

As the primary regulator of p53, the characteristics surrounding the formation of the MDM2-p53 complex are of interest. Crystallographic exploration has revealed the formation of a deep hydrophobic pocket in the NH_2 terminus of the MDM2 phosphoprotein. The binding of p53 to MDM2 takes place within this pocket via the α-helix NH_2 terminal transactivation domain of p53 (Kussie *et al*., 1996). The molecular interaction between MDM2 and p53 is localized to a pocket of 25-109 amino acid residues with hydrophobic properties suited to the amphipathic

nature of the 15 amino acid residue peptides located at the NH_2 terminal domain of MDM2 as well as p53 (Kussie *et al*., 1996; Moll & Petrenko, 2003). The cleft region of MDM2 forms an inward channel of structurally similar sides created by aromatic and 14 hydrophobic residues, consisting of 26-108 amino acids. This enables the tight binding of MDM2 to the transactivation domain of p53 based on the steric complementary of these proteins (Kussie *et al*., 1996; Moll & Petrenko, 2003). The binding site of MDM2 to p53 is confined within the pocket to an 18-26 amino acid region, with particular focus set on the Leu14, Phe19, Leu22, Trp23, and Leu26 residues of p53 as accentuated by the site-directed mutagenesis within this region (Moll & Petrenko, 2003). Residues Phe19, Trp23 and Leu26 configure the α-helix helical hydrophobic domain enabling the MDM2-p53 complex formation by binding into the MDM2 hydrophobic cleft (Kussie *et al*., 1996; Patil *et al*., 2014) (Figure 1.4).

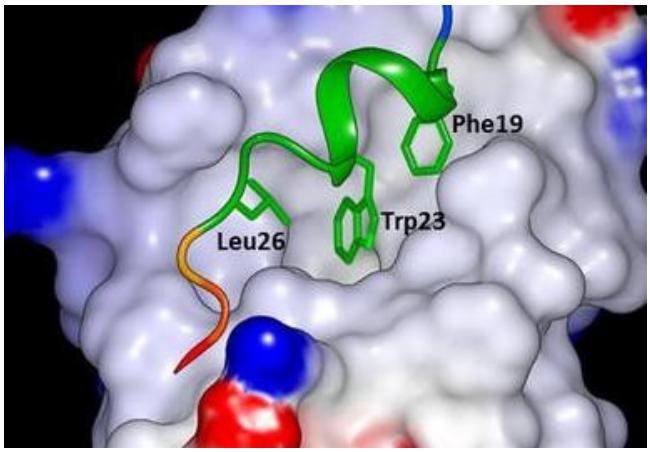

Figure 1. 4: Crystallographic structure of p53 bound to the MDM2 p53-binding site. The MDM2 hydrophobic pocket is seen in grey as the indented, cleft region. The concave structure of MDM2 (covered by the green section represented by p53) substantiates the hydrophobic domain at the NH_2 terminus which forms the binding site for p53. Shown in green are the Phe19, Trp23 and Leu26 amino acids representing the α-helix helical hydrophobic domain that mediates the formation of the MDM2-p53 complex. Adapted from Patil *et al*. (2014).

This interactive domain conforms to a dual-site interface representing a lock and key model (Goh *et al*., 2014). The structural motif created by the amphipathic α-helix domain also suggests binding of the TATA-binding protein associated factors, a diverse class of transactivation factors (Kussie *et al*., 1996). The Phe19, Trp23 and Leu26 binding-centred amino acids particularly participate in the transactivation of p53, concluding that MDM2 inactivates p53 by obscuring the transactivation region of the protein (Kussie *et al*., 1996). Consequently, this interaction of MDM2 with p53 blocks the transcriptional activity of p53 without interacting with the transcriptional machinery, subsequently leading to the ubiquitination of p53 by MDM2, marking p53 for proteasomal degradation (Moll & Petrenko, 2003).

1.5.3 Ubiquitination of p53

It has also been shown that MDM2-mediated p53 ubiquitination is regulated by supplemental proteins. Several studies indicate retinoblastoma binding protein 6 (RBBP6) homologues (P2P-R, RQ1 and PACT) act as a family of proteins known to promote the degradation of p53 through interaction with the p53-MDM2 complex (Franklin, 2000; Hayashida *et al*., 2005; Zitting *et al*., 2002). The determined structure of the MDM2-p53 complex also implies a stability function relating to RBBP6 as a scaffold protein in the formation of this complex (Li *et al*., 2007). This mechanism by which RBBP6 binds the tumour suppressor p53 protein is still insufficiently investigated (Saijo *et al*., 1995; Yoshitake *et al*., 2004; Zhou *et al*., 1999).

RBBP6 functions as a negative regulator of p53 by promoting the degradation of the tumour suppressor protein through ubiquitin-protein ligases or E3 ligases in a similar manner to MDM2 (Pickart, 2001; Pugh *et al*., 2006). The significant effect of RBBP6 on the phenotype of human cancers is denoted in the upregulation of this gene during carcinogenesis, specifically researched in oesophageal and cervical cancers (Chibi *et al*., 2008; Yoshitake *et al*., 2004). The localization of RBBP6 to mitosal chromosomes and nuclear speckles could identify as the main active site for pre-mRNA splicing and processing during interphase, leading to the tumorigenic activity of this protein (Gao *et al*., 2002; Mbita *et al*., 2012; Yoshitake *et al*., 2004). Originally thought to only be of supplementary significance to p53 regulatory function as support for MDM2, RBBP6 has since been identified as a gene supporting tumorigenesis. This essential ability of RBBP6 emanates from the protein's modulation of p53 through cell proliferation properties. Although inadequately researched, the effect of RBBP6 on p53 is noted, but the detailed mechanism of this regulation requires further investigation.

The retinoblastoma protein (pRb) binding domain is situated near the C-terminus of the RBBP6 protein, with an upstream p53 binding domain. RBBP6 is one of the few proteins to interact directly with both p53 and the tumour suppressor pRb, obtruding the binding of p53 to DNA (Simons *et al*., 1997; Witte & Scott, 1997). The interaction of RBBP6 with p53 and pRb is documented in both *in vitro* and *in vivo* studies (Saijo *et al*., 1995; Zhou *et al*., 1999). Despite the obvious potential of RBBP6 as an anti-cancer target, little is known about the full capabilities and associations of this protein. The RBBP6 protein consists of three defining domains, with the RING finger domain being the most significant, located at the N-terminal. This structure indicates pre-mRNA processing protein regulation through covalent modification as specified in MDM2, inciting ubiquitin-dependent degradation of p53 (Pugh *et al*., 2006; Yoshitake *et al*., 2004). Present in all eukaryotic organisms, the presence of the domain with no name (DWNN), located at the N-terminus of the RBBP6 splicing-associated

proteins family, the ubiquitin similar structure of DWNN justifies the ubiquitination modification functionality of RBBP6 (Pugh *et al*., 2006).

1.6 Ezetimibe

Ezetimibe, brand-named Zetia, is a lipid-lowering compound prescribed as a cholesterol-absorption inhibitor for cardiovascular disease treatment. Ezetimibe selectively inhibits the absorption of low-density lipoprotein cholesterol (LDL-C) from the small intestine by binding the critical cholesterol absorption mediator, the Niemann-Pick C1-like 1 (NPC1L1) protein, located in the gastrointestinal tract at the brush border of jejunal enterocytes through oral ingestion (Altmann *et al*., 2004; Bays, 2002; Davis *et al*., 2011; Rosenblum *et al*., 1998). This in turn lowers the available circulating cholesterol. Several pre-clinical models have indicated a reduction in total cholesterol plasma levels as a direct result of ezetimibe (Catapano, 2009). Studies have also proven ezetimibe is most effective in its treatment of hypercholesterolemia when administered in combination with statin therapy (Climent *et al*., 2021; Murphy *et al*., 2016; Phan *et al*., 2012). Side-effects associated with the oral ingestion of ezetimibe include muscle pain, weakness, severe abdominal pain etc. (Altmann *et al*., 2004; Bays, 2002; Davis *et al*., 2011).

1.6.1 Ezetimibe binds to MDM2 *in-silico*

In a study conducted by Twala (2017), several screening methods were employed in an *in-silico* experiment to identify known drugs that could bind to specific structural targets (specifically p53 tumour suppressor regulators MDM2 and RBBP6) and potentially serve as therapeutical agents for cancer. The p53-binding region of MDM2 was investigated for any similar drug matches that were computationally identified for the p53-binding region of RBBP6. In docking the Zinc drug database to the p53-binding domain of MDM2, the software distinguished ezetimibe, binding the drug to the MDM2 hydrophobic cleft with high affinity (Twala, 2017) (Figure 1.5). Interestingly, despite the various similarities in structure, no main compound match was observed between MDM2 and RBBP6 (Twala, 2017).

The database modelled the binding of ezetimibe to the p53-binding site of MDM2. Minimal changes were made to the ezetimibe molecule with the initial formation of a single hydrogen

bond between ezetimibe and the Val93 residue of MDM2 (Twala, 2017). This association is similar to the primary bond formed by the p53 protein to the Trp23 residue of MDM2, as it also binds Phe19, Leu26, and Trp23 upon entering the MDM2 hydrophobic pocket (Twala, 2017) (Figure 1.6 A).

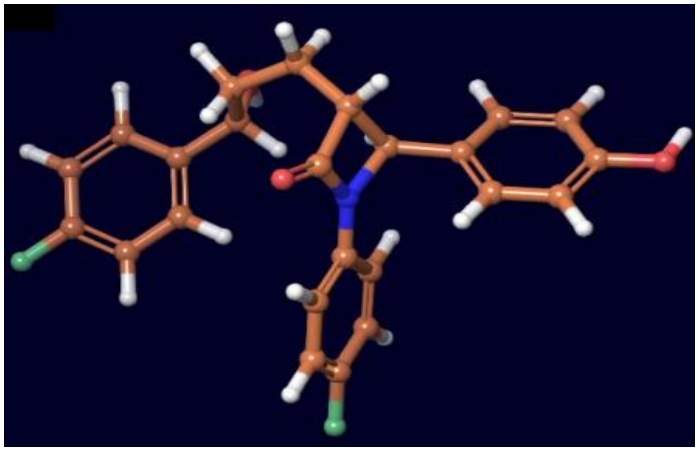

Figure 1. 5: Structure of ezetimibe. A ball-and-stick model of ezetimibe is shown, identified in the ZINC drug database as ZINC03810860. Structurally, ezetimibe ($C_{24}H_{21}F_2NO_3$) indicates nitrogen (N) as a blue sphere, fluorine (F) as single-bound red spheres, oxygen (O_2) as a double-bound red sphere, hydroxide (OH^-) as green spheres, carbon (C) as orange spheres and hydrogen (H^+) as white spheres. Adapted from Twala (2017).

1.6.2 Ezetimibe-MDM2 complex

The stereochemical feasibility and high affinity of the ezetimibe-MDM2 complex are manifested by a multitude of favourable steric contacts (Figure 1.6 B). The diverse structural qualities of ezetimibe coincide with the use of this molecule as an interactive drug. The ligand interaction of ezetimibe ensures the tight binding of the MDM2 p53-binding domain at the 3 Å axis around the drug through hydrophobic and ionic interactions (Twala, 2017) (Figure 1.7). Although structurally accurate, the practical application of ezetimibe in mammalian cells is unknown. The hypothesis of ezetimibe acting as a possible cancer treatment is still untested. Knowing the possible interactions of the various structures involved does however assist in explaining experimental findings.

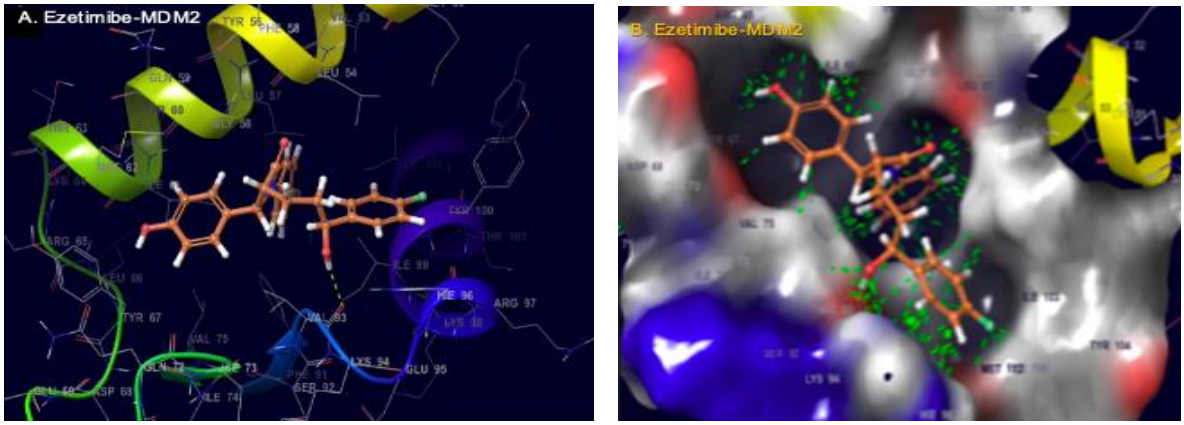

Figure 1. 6: Ezetimibe interaction with the MDM2 p53-binding domain. A: The initial interaction between ezetimibe and the p53-binding domain of MDM2 is shown through a single hydrogen bond with the Val93 residue of MDM2 as indicated by the yellow dotted line. **B:** The interaction between ezetimibe and the p53-binding region of MDM2 with ezetimibe critically binding Phe19, Trp23 and Leu26 residues. This interaction mediates the formation of the ezetimibe-MDM2 complex. The model depicts the MDM2 residue surface created by the hydrophobic domain and the suitable collection of steric contacts shown in green dotted lines of ezetimibe. Adapted from Twala (2017).

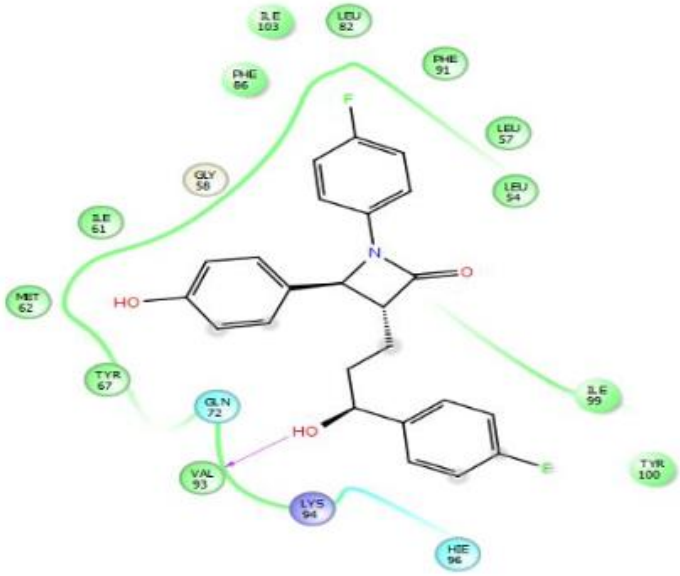

Figure 1. 7: **Ezetimibe 2D ligand interaction with the MDM2 p53-binding domain.** The 2D ligand diagram of ezetimibe interacting with a network of proximal residues located at the hydrophobic cleft region of MDM2 is demonstrated by the green line. The single hydrogen bond is depicted by a purple arrow, signalling the formation of the ezetimibe-MDM2 complex through association with Val93. Adapted from Twala (2017).

1.7 DARTS

The identification of small molecule targets is essential for drug discovery research, metabolomics, proteomics, and chemical genetics. The most common techniques used for

small molecule target identification are associated with affinity chromatography (Ong *et al*., 2012; Ziegler *et al*., 2013). These methods however require the small molecule to be derivatised, which could influence the affinity or the binding accuracy of the molecule. Additionally, the current genetic methods being used are only applicable to specific molecules and the target identification is uncertain, as they rely solely on downstream results (Futamura, 2013). The Drug Affinity Responsive Target Stability (DARTS) technique overcomes these limitations.

1.7.1 Principles of DARTS

The principle of DARTS is that in binding to the small molecule, the target becomes thermodynamically stable. The target proteins, bound to the small molecule, are protected from proteolysis and can be detected compared to degraded peptides (Lomenick *et al*., 2009). The interaction between the targets and the small molecule occurs in compounds with both high- and low affinity. This method is not limited by the chemistry of the target proteins, nor does it require the small molecule to be derivatised or immobilized. Furthermore, DARTS allow for whole-cell lysates to be analysed. This reduces nonspecific interactions between the small molecule and the target proteins, due to the high quantity and variety of proteins in the sample.

1.7.2 Experimental technique of DARTS

DARTS is performed by incubating cell lysate samples with the small molecule of interest and treating the samples with proteases for limited digestion. The cell lysate samples are also treated with a vehicle compound or an inactive analogue, as a control. The samples are separated by sodium dodecyl-sulfate polyacrylamide gel electrophoresis (SDS-PAGE), and the protein bands that are protected by the small molecule from proteolytic digestion are identified. The target proteins in the bands are determined by liquid chromatography-mass spectrometry (LC-MS) (Lomenick *et al*., 2009; Pai et al., 2015). The identification of proteins by gel may be the easiest method, however more efficient non-gel proteomic methods are also compatible with DARTS (Lomenick *et al*., 2011). DARTS is an unbiased method that has been successful in the discovery of unknown targets of various drugs (Lomenick *et al*., 2009; Robinson *et al*., 2013; Sun *et al*., 2014; Tohda *et al*., 2012). Specifically, in a study by Robinson and co-workers (2013), the novel protein targets of disulfiram were identified by DARTS. Disulfiram is an FDA-approved drug developed for the treatment of chronic

alcoholism. DARTS can also be used to screen or validate the targeted binding of small molecules, which has been identified through other techniques (Chen *et al*., 2011). Studies have shown the successful use of DARTS in the verification of recombinant or purified proteins with gel staining, endogenous proteins with western blotting and epitope-tagged proteins with specialised antibodies (Chen *et al*., 2011; Lomenick *et al*., 2009; Robinson *et al*., 2013).

Chapter 2: Project Outline

2.1 Problem Statement

The effect of MDM2 as a negative regular of p53 has been extensively researched. The implication of restricting MDM2 concentrations could hold significant value. While ezetimibe has been shown to bind MDM2 *in-silico*, no experiments have been conducted aiming to prove this computational MDM2-ezetimibe binding complex. The effect of the drug in cancerous cells would be indicative of the effective binding of ezetimibe to MDM2.

The scope of this study is to examine the effect of ezetimibe in cancerous cells and to determine the preliminary formation of the MDM2-ezetimibe complex, as indicated by *in-silico* computational methods.

2.2 Aim and Objectives

This project aimed to determine the cytotoxicity and molecular targets of ezetimibe in cancerous cells. The effects of ezetimibe in both normal and cancer cell lines were tested to investigate the drug as a possible anti-cancer agent. The objectives are as follows:

(i) Determine the cytotoxicity of various ezetimibe concentrations on cancerous and normal cell lines using the MTT assay.
(ii) Determine the cellular characteristics of cancerous cells treated with ezetimibe using flow cytometry.
(iii) Determine the molecular targets of ezetimibe in cancerous cells using DARTS and LC-MS.

Chapter 3: Methodology

3.1 Research Ethics Clearance

Ethical approval for the research was obtained in accordance with the UNISA-CAES Health Research Ethics Committee, with the registration number REC-170616-051.

3.2 Mammalian Cell Culture

Human epithelial lung carcinoma cell line A549, human breast cancer cell line MCF-7, and immortalized human embryonic kidney cell line HEK293 were used in this study. The A549 cells were purchased from Separation Scientific, SA. HEK293 and MCF-7 cells were a kind gift from Dr Jitcy Saji Joseph (National Institute for Occupational Health).

3.2.1 Recovery of cells from frozen stocks

The frozen cell vials were removed from the -80 °C freezer and thawed at 25 °C. Once thawed, the outer surface of the vials was cleaned with 70% ethanol and the cells were transferred to a T25 culture flask containing 5 ml of recovery media (20% fetal bovine serum (FBS), 1 % penicillin-streptomycin, 79% DMEM media with L-Glutamine). The T25 culture flask containing the cells was incubated at 37 °C with 5% CO_2 in a humidified incubator. Cells were incubated until a confluency of 80-90% was reached.

3.2.2 Sub-culture

Once confluency of 80-90% was reached, the cells were passaged routinely for further experiments. The recovery media in the T25 culture flask was discarded. The recovered cells attached to the base of the flask were washed with 3 ml phosphate-buffered saline (PBS), pH 7.5. This step was repeated to ensure all media were removed from the cells before the trypsin-EDTA treatment. Thereafter, 3 ml of 1 X trypsin-EDTA was added to the flask and the flask was incubated at 37 °C for 5-20 minutes to assist in cellular detachment. The

trypsinization time varied for each cell line. HEK293 trypsinized for approximately 5 minutes. A549 and MCF-7 trypsinized for approximately 10 minutes. Once detached, 3 ml of pre-warmed maintenance media (10% FBS, 1% penicillin-streptomycin, 89% DMEM media with L-Glutamine) was added to the flask to stop the trypsin-EDTA protein degradation reaction. The cell solution was then decanted into a sterile 15 ml tube and centrifuged at 1000 *x g* for 3 minutes. The supernatant was discarded, and the cell pellet was resuspended in 1 ml of fresh pre-warmed maintenance media. The resuspended cell solution was then distributed to a new T75 culture flask containing 10 ml of maintenance media for further sub-culturing. The cells were then incubated at 37 °C with 5% CO_2 in a humidified incubator. Alternatively, the cells were counted for experimentation as described in section 3.1.3.

3.2.3 Cell counting

The cells were counted using a hemocytometer. The resuspended cell solution was further diluted with pre-warmed maintenance media. Thereafter, 10 µl of the cell suspension was transferred to an Eppendorf tube containing 10 µl of 0.4 % trypan blue solution. The cells and the stain were mixed thoroughly and allowed to stand for 5 minutes. The coverslip was placed on the hemocytometer, and the trypan blue-cell suspension mixture was added to the chambers of the hemocytometer with a pipet. The cells were counted in the four 1 mm corner squares. Cells that touched the top and left line of the perimeter of the squares were counted. Cells that touched the bottom and right perimeter of the squares were not counted. Additionally, non-viable cells were stained blue. The number of cells per ml was determined by the following calculation:

$$\text{Number of cells per ml: } \frac{\text{average count per square} \times 10^4 \times \text{dilution factor}}{\text{number of squares counted}}$$

The average number of cells counted per square was calculated for the 4 squares counted. The 10^4 value represents the total volume of each square of 0.1 mm^3 or 10^{-4} cm^3. The dilution factor is 2 based on the two-fold dilution of the cell suspension with the trypan blue, which reduced the original concentration of the suspension by half. The number of squares counted was four. Only the viable cell count was used to determine the number of cells per ml.

3.2.4 Storage of cells

Once confluency of 80-90% was reached, the maintenance media in the T75 culture flask was discarded. The cells attached to the base of the flask were washed, twice, with 5 ml PBS, pH 7.5. The cells were trypsinized with 5 ml of 1 X trypsin-EDTA. The flask was incubated at 37 °C for 10-20 minutes to assist in cellular detachment. Once detached, the trypsin was neutralized by resuspending the cells in 5 ml of pre-warmed maintenance media. The cell solution was then decanted into a sterile 15 ml tube and centrifuged at 1000 *x g* for 3 minutes. The supernatant was discarded, and the cell pellet was resuspended in 4 ml of freezing media (10% DMSO, 90% FBS). The cellular resuspension was aliquoted into sterile cryovials containing 1 ml of the cell solution each. The cells were frozen at -80 °C.

3.3 Drug Treatment

The drug treatment of cell lines A549, MCF-7, and HEK293 was done uniformly. The drug agent, ezetimibe, was introduced to the cell lines in a variety of concentrations to establish the effect of the drug in human lung cancer cells (A549), human breast cancer cells (MCF-7), and human embryonic kidney cells (HEK293). The ezetimibe powder was purchased from Sigma-Aldrich, SA.

The cell lines were cultured as mentioned above. The collected cell pellet was resuspended in 1 ml of fresh pre-warmed maintenance media and the cells were counted as described in section 3.1.3. The cells were seeded according to experimental requirements and incubated for 12-16 hours to allow for attachment in maintenance media. Once attached, the maintenance media was removed, and replaced with fresh media (DMEM) containing various concentrations of ezetimibe ranging from 10 µM to 80 µM. The cells were incubated for 48 hours at 37 °C with 5% CO_2 in a humidified incubator. Following the incubation with the drug (48 hours), floating cells were collected by decanting the media into a sterile 15 ml tube and centrifuging at 1000 *x g* for 5 minutes. Any remaining attached cells were collected by trypsinization. The dead floating cells and the live trypsinized cells from each plate were combined and the cells were pelleted via centrifugation at 1000 *x g* for 5 minutes. Dead and live cells were collected for experimentation to ensure unbiased results.

Controls included untreated cells, where ezetimibe was substituted with DMEM. The untreated controls served as a reference guide against the treated samples. Vehicle controls included cells treated with ethanol, which is the vehicle medium used to dilute the powdered ezetimibe drug. Vehicle controls with ethanol were treated at the highest drug concentrations, 80 µM. This determined any effect that the vehicle may have on the cells that could influence ezetimibe-treated results.

3.4 MTT Assay

The MTT assay measured the cytotoxicity of various ezetimibe concentrations on human lung cancer cells (A549), human breast cancer cells (MCF-7), and human embryonic kidney cells (HEK293). The MTT assay is a colorimetric assay, used to assess cellular metabolic activity via NADPH-dependent cellular oxidoreductase enzymes. When introducing MTT to cell samples, the yellow tetrazole was reduced to purple formazan in living cells. The visible colour change indicated the viability of the cells based on exposure to different concentrations of ezetimibe. The cellular viability was quantified by measuring the absorbance of the solution at a certain wavelength (570nm) via a spectrophotometer.

Cell pellets from each respected cell line were resuspended in maintenance media and 50 µL of the cell solution was added to each well of the 96-well MTT plate. Each 50 µL of the cell solution contained 5000 cells. The cells were incubated for 12-16 hours at 37 °C with 5% CO_2 in a humidified incubator to allow for attachment. Thereafter, 50 µL of various ezetimibe drug concentrations were added, ranging from 10 µM to 80 µM. The cells were incubated for 48 hours at 37 °C with 5% CO_2 in a humidified incubator. Following drug treatment, 10 µL of MTT was added to every well and the cells were incubated for 4 hours at 37 °C with 5% CO_2 in a humidified incubator. Thereafter, 100 µL of DMSO was added to every well to solubilize the formazan crystals. The cells were incubated for 5 minutes at 37 °C with 5% CO_2 in a humidified incubator. The MTT plate was analysed by the Varioskan Flask Microplate Reader (Thermo Fisher).

3.4.1 Experimental replicates

The results of the MTT assay averaged data points from three biological replicates conducted within the experiment and three technical replicates across experiments. The statistical outliers for replicates within each experiment were determined by the interquartile range (IQR) of the data points. The data points were categorised from low to high, where the lowest value represents the first quartile (Q1), the middle value represents the median, and the highest value represents the third quartile (Q3). The quartile values were calculated within the 25^{th} percentile of the categorised data points. Thereafter, the interquartile range (IQR) was determined by subtracting the first quartile (Q1) from the third quartile (Q3) e.g., IQR = Q3 – Q1. The upper limit for the statistical outliers was determined by the sum of the third quartile (Q3) and the multiplication of 1.5 with the interquartile range (IQR) e.g., upper limit = Q3 + (1.5 x IQR). Similarly, the lower limit for the statistical outliers was determined by subtracting the first quartile (Q1) from the multiplication of 1.5 with the interquartile range (IQR) e.g., lower limit = Q1 - (1.5 x IQR). The measurements that fell outside of these parameters were eliminated from the processed data. These statistical calculations were done on all three biologically replicated experiments, the results were averaged and presented graphically in figure 4.1 and figure 4.2. The variability within the data sets was calculated and displayed visibly in figure 4.1 with added standard deviation bars. The calculations and schematics were done in Microsoft Excel.

3.4.2 Statistical analysis

The statistical analysis was done with GraphPad Prism 9 software. The mean values ± SD (standard deviation) were determined for the three biological replicates conducted within the experiment and three technical replicates across experiments, listed in Table A8. The error bars represent the standard error of the mean between the biological replicates. The student t-test compared two sets of data, specifically HEK293 vs MCF-7 and HEK239 vs A549, for each individual concentration. P-value < 0.05 was considered statistically significant. The $p \leq 0.0001$ (****), $p \leq 0.001$ (***) and $p \leq 0.01$ (**) values were considered statistically significant, while $p \geq 0.05$ was not considered statistically significant. The determined p-values were listed in Table A9.

The results of the MTT assay were also used to determine ezetimibe's half-maximal inhibitory concentration (IC_{50}) on the drug-treated cell lines. The IC_{50} indicates the concentration of an antagonist drug needed to inhibit a biological process by half, providing a measure of the drug's potency. The IC_{50} values were calculated by linear approximation regression of the cellular viability percentages. The data points were plotted against the tested drug

concentrations. A trendline was drawn over the data points and the configuration of the linear equation y=mx+c, where y=50 and x=IC_{50}, provided the ezetimibe concentration needed to half the viable cell population. These IC_{50} values determined the drug concentrations used in future experiments to ensure the optimal potency of ezetimibe on the tested cell lines.

3.5 Flow Cytometry

Human lung cancer cells (A549) and human embryonic kidney cells (HEK293) were used for flow cytometry analysis. Human breast cancer cells (MCF-7) were excluded based on the minimal effect of ezetimibe on these cells, demonstrated by the MTT assay results. Concentrations below and above the IC_{50} value of 40 µM (as determined by the MTT assays) were chosen for investigation, specifically 20 µM and 60 µM.

Drug-treated HEK293 and A549 cell lines were counted as described in section 3.1.3. The cells were seeded into 6-well cell culture plates with 300 000 cells per well. Each well contained 2 mL of maintenance media. The cells were incubated for 12-16 hours at 37 °C with 5% CO_2 in a humidified incubator to allow for attachment. Thereafter, the maintenance media was removed without disturbing the attached cells. Ezetimibe drug concentrations of 20 µM, 40 µM, and 60 µM in DMEM media were added as 2 mL per well. The cells were incubated for 48 hours at 37 °C with 5% CO_2 in a humidified incubator. Following drug treatment, dead cells were collected by pipetting the 2 mL of media into marked sterile 15 ml tubes. The samples were kept independently per well. Live cells attached at the bottom of the 6-well cell culture plates were washed twice with PBS before being trypsinized. After trypsinization, the cells were collected in the marked sterile 15 ml tubes containing the dead cells. Dead and live cells were collected from the same well, to ensure unbiased results. The tubes were centrifuged at 1000 *x g* for 3 minutes. The supernatant was discarded, and the cell pellet was washed with cold PBS. The tubes were centrifuged at 1000 *x g* for 3 minutes, the supernatant was discarded, and the cell pellet was treated for apoptosis or cell cycle analysis experiments.

The BD FACSAria™ III Cell Sorter was used for both cycle analysis and apoptosis analysis. Configuration checks were run on the BD FACSAria™ III Cell Sorter before each analysis to ensure optimal performance over time. System configurations included establishing a stable drop pattern of the transport droplets displayed as the breakoff stream. The parameters for the correct drop pattern were determined by BD Biosciences (2012). The CS&T beads (bright

to dim beads dyed with fluorochromes) were also used during configurations to define the analysis baseline. Thereafter, analysis was initiated and the application settings were optimized. Firstly, the analysis results were populated on a dot graph with forward scatter (FSC) on the x-axis and side scatter (SSC) on the y-axis. Adjustments were made to the FSC and SSC voltages to place the population of interest in a diagonal projection. Secondly, FSC area scaling was done and assessed in the statistical views of a histogram, matching the FSC-Area signal to the FSC-Height signal. Finally, the FSC threshold value was optimised to eliminate debris displayed on the left corner of the graph. Once optimized, the application setting remained constant throughout the experiment. The complete application setup and sample analysis were done as per the BD Biosciences (2012) guidelines.

3.5.1 Apoptosis

The proliferation of the cell samples was determined by flow cytometry based on apoptosis analysis. The process of apoptosis is identified through cellular characteristics. One of the earliest indicators of this programmed cell death is the translocation of the phospholipid phosphatidylserine (PS) membrane from the inner to the outer membrane leaflet, externalizing PS to the cell's environment. This process was visualized using Annexin V-FITC (Sigma-Aldrich). Annexin V is a Ca^{2+}-dependent phospholipid-binding protein with a high affinity for PS. This affinity is maintained even when conjugated to the FITC fluorochrome. The Annexin V-FITC stain serves as a probe-sensitive detection method for early-stage cellular apoptosis. Apoptotic identification was enhanced by adding propidium iodide (PI) vital dye (from Invitrogen). PI is a red-fluorescent dye that binds to nucleic acids. Live cells and apoptotic cells are thus impermeable to PI as the DNA is still within the cellular nucleus. PI solely stains cells in late-stage apoptosis or necrosis, which exposes DNA to the cell's environment upon death. The loss of cell membrane permeability detected by PI is a hallmark of necrosis and late-stage apoptosis.

The drug-treated cell pellets were resuspended in 100 µL of 1 x Annexin-binding buffer. The 5 x Annexin-binding buffer consisted of 50 mM HEPES, 700 mM NaCl, and 12.5 mM $CaCl_2$ with pH 7.4. The 1 x Annexin-binding buffer was diluted as one part of the 5 x Annexin-binding buffer and four parts of distilled water. Thereafter, 5 µL of Annexin V-FITC and 1 µL of 100 µg/mL PI working solution were added to the cellular solution. The 100 µg/mL PI working solution consisted of 5 µL 1mg/mL PI stock solution diluted in 45 µL 1 x Annexin-binding buffer. The cellular solution was gently vortexed followed by 15 minutes of incubation at 25 °C in the

dark. Following incubation, 400 µL of 1 x Annexin-binding buffer was added to each tube. Analyses by the BD FACSAria™ III Cell Sorter using 488-nm excitation commenced within one hour.

3.5.1.1 Experimental replicates

The configuration checks and application settings of the BD FACSAria™ III Cell Sorter were optimized before each analysis as described in section 3.4. Three biological replicates were conducted within the experiment. The BD FACSDiva software was used for apoptosis data analysis. The results were populated on a dot graph with Alexa Fluor 488-A (represents Annexin V-FITC) over PerCP-Cy5-5-A (represents PI). The graph was gated (directed by the data pattern) into four quadrants at the 10^3 intersections. The statistics were configured, including the number of events and the quadrant populations. The recorded events per sample were 20 000 – 50 000 depending on the cell density. The parent cell population refers to the cells gated during the data analysis. The total cell population refers to all the cells recorded in the sample, including cells not gated. The parent cell population and the total cell population were the same. This indicates total sample analysis for unbiased results during data collection.

3.5.1.2 Statistical analysis

The statistical analysis was done with GraphPad Prism 9 software. The mean values ± SD (standard deviation) were determined for the three biological replicates conducted within the experiment and three technical replicates across experiments, listed in Table A8. The error bars represent the standard error of the mean between the biological replicates. The student t-test compared the untreated A549 cells to the treated A549 cells for each stage of apoptosis. P-value < 0.05 was considered statistically significant. The $p \leq 0.0001$ (****), $p \leq 0.001$ (***) and $p \leq 0.01$ (**) values were considered statistically significant, while $p \geq 0.05$ was not considered statistically significant (ns). The determined p-values were listed in Table A9.

3.5.2 Cell Cycle Analysis

Flow cytometry quantitatively determines the percentages of a cell population in various phases of the cell cycle. During cell cycle analysis, highly fluorescent signals are produced

when PI intercalates into the major groove of DNA. Treatment with RNaseA was necessary to distinguish between DNA and RNA staining.

The drug-treated cell pellets were gently resuspended in 400 µL of cold PBS, thereafter 800 µL of cold 100% ethanol was slowly added to the suspension. The cell suspension was mixed well and incubated at -20 °C for two weeks. Following incubation, the prepared cells equilibrated at 25 °C and were gently resuspended. The tubes were centrifuged at 500 *x g* for 5 minutes and the supernatant was discarded without disrupting the cell pellet. The cell pellets were washed by resuspension in 1 mL of PBS and centrifugation at 500 *x g* for 5 minutes. The supernatant was discarded, and the cell pellet was resuspended in 200 µL Propidium Iodide + RNase Staining solution. The Propidium Iodide + RNase Staining solution consisted of 9.45 mL PBS, 500 µL 20x PI (1mg/mL), and 50 µL 200x RNaseA (110 000 U/mL). Thereafter, the cell solution was gently vortexed and incubated for 30 minutes at 37 °C in the dark. The samples were kept on ice in the dark and analysed by the BD FACSAria™ III Cell Sorter using 488-nm excitation within one hour.

3.5.2.1 Experimental replicates

The configuration checks and application settings of the BD FACSAria™ III Cell Sorter were optimized before each analysis as described in section 3.4. Three biological replicates were conducted within the experiment. The FlowJo software was used for cell cycle data analysis. The data was gating automatically by the software to remove any possible biased data editing. The automated gating was analysed to ensure accuracy, with no changes required or implemented. The Dean-Jett-Fox model was applied to quantify the percentage of the cell population in the distinct phases of the cell cycle (Fox, 1980). The software categorises the cell cycle phases as G1, S and G2, however, it should be noted that these phases have not been specifically distinguished. The more accurate description for the phases would be G0/G1, S and G2/M.

3.5.2.2 Statistical analysis

The statistical analysis was done with GraphPad Prism 9 software. The mean values ± SD (standard deviation) were determined for the three biological replicates conducted within the experiment and three technical replicates across experiments, listed in Table A8. The error bars represent the standard error of the mean between the biological replicates. The student

t-test compared the untreated A549 cells to the treated A549 cells for each stage of cell cycle recorded. P-value < 0.05 was considered statistically significant. The $p \leq 0.0001$ (****), $p \leq 0.001$ (***) and $p \leq 0.01$ (**) values were considered statistically significant, while $p \geq 0.05$ was not considered statistically significant. The determined p-values were listed in Table A9.

3.6 DARTS

DARTS was used to identify the potential protein targets of ezetimibe. The technique is based on the principle that a protein structure stabilizes upon binding to a small molecule drug. In binding to the drug, the target proteins exhibit resistance to protease degradation. The degradation of proteins not bound to the drug will not be affected (Lomenick *et al*., 2011). The procedure is conducted by treating aliquots of cell lysate with the compound of interest followed by the limited digestion of proteins in the samples with proteases. Experimental control samples substituted the compound of interest with the ethanol vehicle. The samples are separated by SDS-PAGE and stained to exhibit protein bands that are protected from proteolysis. Mass spectrometry (MS) is subsequently used to identify the proteins in the selected band.

3.6.1 Small molecule binding and protein digestion

The concentration of the small molecule (ezetimibe) used in this experiment relates to the response concentration of the drug. Ezetimibe evoked a response in A549 cells at 10 µM, as indicated by the MTT assay. This is only indicative of the binding affinity of the drug, as the targets are unknown. The 100 µM concentration used was taken as 10-fold higher than the 10 µM response concentration, as suggested by Lomenick and co-workers (2011).

DARTS was performed according to the method outlined by Lomenick and co-workers (2011). A549 cells were cultured in a T75 culture plate, the cells were collected and pelleted without ezetimibe drug treatment. The cell pellet was washed by resuspension in 1 mL of PBS and centrifugation at 500 *x g* for 5 minutes. The supernatant was discarded, and the cell pellet was resuspended in 650 µL of a non-denaturing lysis buffer. The lysis buffer consisted of 958 µL 2 x Triton-X Lysis buffer (0,4% Triton-X 100, 400 mM NaCl, 100 mM Tris-HCl with pH 7.5, and 20% glycerol), 2 µL 1 M NaF solution, and 40 µL Pronase (10 mg/ml) (Sigma-Aldrich) solution. Following incubation, the cell lysate was centrifuged at 18 000 *x g* for 10 minutes at 4 °C.

Thereafter, 600 µL of the supernatant was transferred to a new sterile Eppendorf tube. To the supernatant, 66,7 µL of 10 x TNC buffer was added. The 10 x TNC buffer consisted of 500 mM Tris-HCl (pH 8.0), 500 mM NaCl and, 100 mM $CaCl_2$. The mixture was split into two sterile Eppendorf tubes, each containing 300 µL of the cell lysate. The one tube acted as the control sample, wherein 3 µL of the ethanol vehicle (100 µM) was added. The second tube acted as the treated sample, wherein 3 µL of ezetimibe (100 µM) was added. Both samples were mixed gently and incubated for 1 hour at 25 °C. The control and the treated sample tubes were split into 6 tubes respectively, with each new tube containing 50 µL of the protein lysate. Thereafter, the protein lysates were proteolyzed by treating the tubes with different concentrations of pronase. The 1:100 pronase stock solution (1.25 mg/ml) was made by adding 87.5 µL cold 1 x TNC buffer to 12.5 µL of pronase (10 mg/ml). The 1 x TNC buffer consisted of 10 µL 10 x TNC buffer and 90 µL of distilled water. Serial dilution of the 1:100 pronase stock solution was made with 1 x TNC buffer to create 1:300, 1:500, 1:1000 and, 1:3000 solutions. The dilutions were added as 2 µL per tube, at 1-minute intervals exactly. The 5 dilutions (1:100, 1:300, 1:500, 1:1000, 1:3000) were added to 5 of the 6 tubes for both the control samples and the treated sample. The final tube served as the non-digested control. The samples were incubated for exactly 30 minutes at 25 °C following pronase treatment. The reaction was stopped by adding 18 µL of sample buffer to each tube. The sample buffer consisted of 12% SDS, 30% glycerol, 6% β-Mercaptoethanol, 0.05% Coomassie Brilliant Blue, and 150 mM Tris-HCl with pH 7.0. The sample buffer was added at 1 minute to ensure an incubation time of exactly 30 minutes. Thereafter, all the samples were incubated for 3 minutes at 95 °C before SDS-PAGE analysis.

3.6.2 SDS-PAGE

SDS-PAGE analysis was used to separate the digested proteins in the samples according to size. The SDS-PAGE gels were prepared as indicated in table 3.1. with a 12% separating gel directly overlayed with a 4% stacking gel. The gels were mounted in the vertical electrophoresis apparatus (Bio-Rad). The anode and cathode buffers were added respectively, prepared as indicated in table 3.2. Following incubation, 16-20 µL of each sample was loaded onto the gel, as well as the SuperSignal™ Enhanced Molecular Weight Protein Ladder (Thermo Scientific) to indicate the size of separated protein bands. The Tricine-SDS-PAGE method was used for analysis (Schägger, 2006). The initial 40 voltage was set until the sample completely entered the separating gel, thereafter it was gradually increased to 90 V until the end of the run. The SDS-PAGE gels were stained overnight in Coomassie Blue stain

and destained for 1 day with SDS-PAGE destain. The Coomassie Blue stain consisted of 250 mL of 50% methanol, 0.25g Coomassie Brilliant Blue, 50 mL acetic acid, and 200 mL of distilled water. The SDS-PAGE destain consisted of 50 mL ethanol, 70 mL acetic acid, and 880 mL distilled water. Thereafter, the gels were visualized using the GelDoc Imaging System (Bio-Rad).

Table 3. 1: SDS-PAGE Gel Composition

Reagent	4% Stacking gel	12% Separating gel
Acrylamide/-Bis-acrylamide (30%)	660 µL	4 ml
Gel buffer (3X)	760 µL	5 ml
Glycerol	_	500 µL
Distilled water	3.42 ml	340 µL
APS (10%)	150 µL	100 µL
TEMED	5 µL	6 µL

Table 3. 2: SDS-PAGE Buffers Composition

Reagent	Anode Buffer (10X)	Cathode Buffer (10X)	Gel Buffer (3X)
Tris	1 M	1 M	3 M
Tricine	_	1 M	_
SDS	_	1%	0.3%
HCl	0.225 M	_	1 M
pH value	8.9	8.3	8.5

3.6.3 Mass Spectrometry

The SDS-PAGE gel image visualised the absent protein bands in the vehicle-treated samples, compared to bands present in the drug-treated samples. The expected protein to bind to ezetimibe was MDM2, with a calculated molecular weight of 55 kDa and a predicted SDS-PAGE molecular weight of up to 90 kDa. Regardless of this expectation, bands were visible in the ezetimibe-treated sample proximate to the 50 kDa mark that was absent in the vehicle-treated sample. The visible bands were cut from the gel with a sterile scalpel and placed in 10% ethanol. The gel samples were stored at -20 °C before being expertly analysed by Dr Previn Naicker (CSIR Nextgen Health).

3.6.3.1 Protein digestion

The proteins were digested from the gel bands according to Shevchenko *et al*., (2006). The proteins in the gel were reduced with 10 mM DTT in 25 mM ammonium bicarbonate for 1 hour at 60 °C. The samples were cooled to 25 °C and 100% acetonitrile was added. After 10 minutes of incubation, the supernatant was discarded and 55 mM iodoacetamide in 25 mM ammonium bicarbonate was added. The sample was incubated for 20 minutes at 25 °C in the dark. The supernatant was discarded and the gel pieces were hydrated with 25 mM ammonium bicarbonate in 50% acetonitrile. The sample was vortexed and the supernatant was removed. The gel pieces were dried and trypsin was added before overnight incubation at 37 °C. The protein digestion was stopped by adding 0.1% formic acid. The samples were dried under a vacuum and re-suspended in 2% acetonitrile and 0.2% formic acid for LC-MS analysis.

3.6.3.2 LC-MS analysis

Digested peptides were analyzed using a Dionex Ultimate 3000 RSLC liquid chromatography (LC) system. The LC system was coupled to an AB Sciex 5600 TripleTOF mass spectrometer. The peptides were injected into the LC-MS system and de-salted inline by an Acclaim PepMap C18 column (75 µm × 2 cm) for 2 min at a flow rate of 5 µl per min^{-1} with 2% of acetonitrile and 0.2% of formic acid). The gradient elution was created with 6-40% of acetonitrile and 0.1% of formic acid over 15 minutes assisted in dislodging possibly trapped peptides. Thereafter, the peptides were separated on a C18 Waters nanoEase CSH column (75 µm × 25 cm, 1.7 µm particle size) at a flow rate of 0.3 µl per min^{-1}. The data-dependent acquisition was used, with precursor (MS) scans from *m/z* 400-1500 (2^{+}-5^{+} charge states) taken in 100 milliseconds, followed by 40 fragment ion (MS/MS) scans from *m/z* 100-1800, each taken in 25 milliseconds.

3.6.3.3 Data analysis

Protein Pilot V5.0 software (SCIEX) was used for data analysis. The software database contained sequences from *Homo sapiens* downloaded from UniProt (Swiss-Prot on 1 October 2022) and common contaminants. The search parameter set trypsin as the digestion enzyme, and cysteine alkylation (iodoacetamide) as a fixed modification and allowed biological modifications. Peptides with a single hit as evidence for the protein hit (minimum confidence

score of 95) were removed. Additionally, proteins were filtered according to size from 45 – 55 kDa for sample 1 and below 50 kDa for sample 2. The keratin-linked protein, likely to have been introduced during sample preparations, and some housekeeping genes were removed.

Chapter 4: Results

This study aimed to investigate the cytotoxic effect and molecular targets of ezetimibe in A549 lung cancer cells. Cytotoxicity was measured using MTT assays and demonstrated that ezetimibe is toxic in A549 cells and less toxic in MCF-7 and HEK293 cell lines. Furthermore, molecular underpinnings of ezetimibe were investigated through flow cytometry, specifically by focusing on apoptosis and cell cycle analysis experiments. Apoptosis analysis quantified the cell population in various stages of apoptosis while cell cycle analysis determined the effect of ezetimibe on the different phases of the cell cycle, thereby providing an insight into the potential molecules affected. Both p53 and MDM2 are involved in specific phases of the cell cycle. Finally, the molecular targets of ezetimibe were determined with DARTS and LC-MS. Even though the expected MDM2 molecule was not found in these samples, the proteins that were identified could be potential targets of ezetimibe providing insights into the pathways that may be influenced by this drug.

4.1 Cytotoxic effect of ezetimibe

4.1.1 MTT Assay

MTT assays evaluated the cytotoxic ability of ezetimibe in human breast cancer cells (MCF-7), human lung cancer cells (A549), and human embryonic kidney cells (HEK293). The cellular viability of these cell lines was estimated after 48 hours of drug treatment with ezetimibe concentrations of 10 µM, 20 µM, 30 µM, 40 µM, 60 µM, and 80 µM. The untreated samples provided a reference from which drug-treated samples could be measured. The ethanol vehicle showed results similar to that of the untreated samples, indicating no significant effect on any of the cell lines tested. Figure 4.1 demonstrates that ezetimibe is toxic to the A549 cells and not toxic to the normal cell line and MCF-7 cells at the same concentrations.

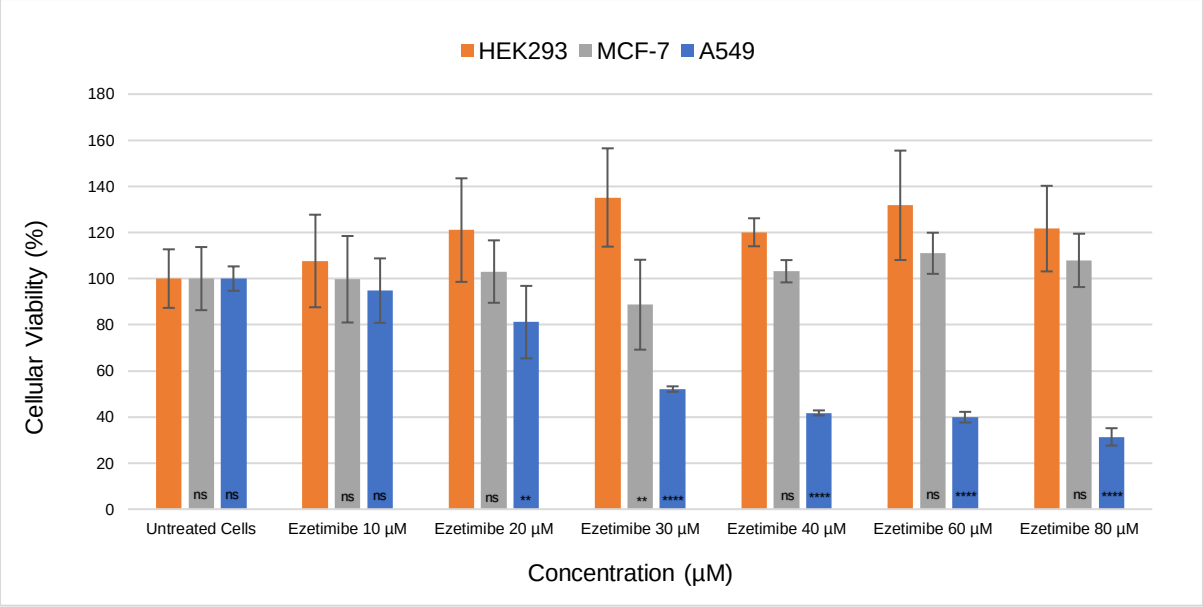

Figure 4. 1: **The cytotoxicity of ezetimibe.** The MTT assay data of HEK293, MCF-7, and A549 cell lines treated for 48 hours with ezetimibe concentrations of 10 µM, 20 µM, 30 µM, 40 µM, 60 µM, and 80 µM. The cytotoxic effect of ezetimibe is seen in A549 cells with a decrease in cellular viability over increased concentrations. Ezetimibe proves non-toxic to HEK293 and MCF-7 throughout varying concentration levels. The experimental data compared MCF-7 and A549 to HEK293, within each concentration. The data were considered statistically significant when the p-value was ≤ 0.05. The $p \leq 0.0001$ (****), $p \leq 0.001$ (***) and $p \leq 0.01$ (**) values were considered statistically significant, while $p \geq 0.05$ was not considered statistically significant (ns). Section 3.4.2 shows the calculated statistical analysis.

Cellular growth variability between the data sets showed different growth rates for the HEK293 cell line specifically. While slight growth variations between the biological replicates were observed for HEK293, the high percentage of HEK293 cellular viability was consistent.

The IC_{50} values were calculated by linear approximation regression of the cellular viability percentage shown in figure 4.1. A trendline was drawn over the data points and the configuration of the linear equation ($y=mx+c$, where $y=50$ and $x=IC_{50}$) provided the ezetimibe concentration needed to half the viable cell population. The data points were plotted against the tested drug concentrations as presented in figure 4.2. The calculated IC_{50} values are shown in table 4.1.

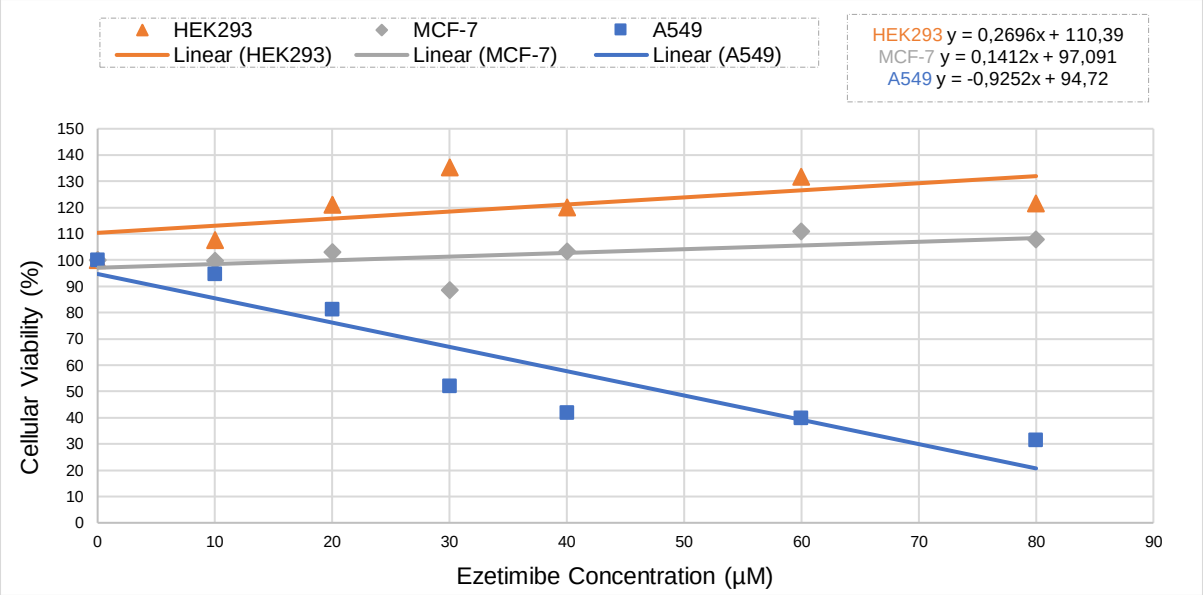

Figure 4. 2: **Linear MTT IC_{50} assay.** The linear representation of the MTT assay data points of HEK293, MCF-7, and A549 cell lines treated for 48 hours with ezetimibe concentrations of 10 µM, 20 µM, 30 µM, 40 µM, 60 µM, and 80 µM. Ezetimibe has a toxic effect on A549 cells with increased concentrations, while the drug proves non-toxic to HEK293 and MCF-7 cells at these increased concentrations.

Table 4.1 shows the calculated IC_{50} values for HEK293, MCF-7 and A549 cell lines treated with ezetimibe. This shows that ezetimibe kills A549 at a concentration almost 5-fold lower than HEK293 and 7-fold lower than MCF-7. These values verify that ezetimibe is not cytotoxic to human embryonic kidney cells. It also proves its cytotoxicity in human lung cancer cells and its ineffectiveness in human breast cancer cells.

Table 4. 1: IC_{50} values of ezetimibe

	IC_{50}
HEK293	224 µM
MCF-7	334 µM
A549	48 µM

4.2 Molecular mechanisms underpinning the anticancer cytotoxicity of ezetimibe

The cytotoxicity of ezetimibe evaluated in the MTT assay established that ezetimibe is selectively toxic to certain cancer cells. Since ezetimibe has proven ineffective in killing either HEK293 or MCF-7 cells, these cell lines were excluded from additional experiments. The

systematic actions and targets of the drug were evaluated in A549 cells due to its proven interaction with ezetimibe. The IC_{50} values calculated for A549 cells set the optimal ezetimibe concentration for flow cytometry and DARTS analysis at 40 µM, with the marginal concentration of 20 µM and 60 µM.

4.2.1 Apoptosis

The process of apoptosis is characterized by distinct morphological features and biochemical mechanisms. The morphology of early-stage apoptosis cells includes cellular shrinking and pyknosis (Kerr *et al*., 1972). Cell shrinkage reduces the cell size (presented as irregular cell outlines) and condenses the organelles, while pyknosis is caused by the condensation of chromatin. Thereafter, plasma membrane blebbing is followed by karyorrhexis and the apoptotic bodies are phagocytosed (Elmore, 2007). Hallmarks of the progression of apoptosis are early-stage marginalization (1); nucleic acid fragmentation (2); organelle displacement (3); distinct vacuoles (4); and plasma membrane blebs (5) (White & Cinti, 2004). The early stages of apoptosis involve indicative changes to the cell membrane. These changes were visualized by fluorochrome. Similarly, the late stages of apoptosis or necrosis are distinguished by DNA fragmentation before phagocytoses, these nucleic acid fragments were stained and visualized by fluorescent dye.

Cellular apoptosis was visualized by exposing drug-treated A549 cells to Annexin V-FITC and PI. Live cells appeared Annexin V-FITC and PI negative, suggesting intact plasma membranes. Early-stage apoptotic cells appeared Annexin V-FITC positive and PI negative, signalling PS exposure with membrane integrity enclosing cellular DNA. Late-stage apoptotic or necrotic cells appeared Annexin V-FITC and PI negative, suggesting complete cellular rupture.

Figure 4.3 shows the distribution of the A549 cell population treated with various ezetimibe concentrations introduced to Annexin V-FITC and PI. The Alexa Fluor 488-A designated to the x-axis represents Annexin V-FITC while PerCP-Cy5-5-A designated to the y-axis represents PI. The cell population was distributed into defined quadrants. Based on this distribution, quadrant 1 (Q1) represented in orange, shows completely impaired cells without intact cell membranes to display PS proteins while exposing cellular DNA within. Cells in Q1 presented negative for Annexin V-FITC and positive for PI. Quadrant 2 (Q2), represented in red, shows ruptured cells in late-stage apoptosis or necrosis exposing the cell membrane PS proteins and cellular DNA within Cells in Q2 presented positive for both Annexin V-FITC and

PI. Quadrant 3 (Q3) represented in green, shows the live cells that maintained cell membranes impermeable to either Annexin V-FITC or PI. Quadrant 4 (Q4), represented in blue, shows cells in early-stage apoptosis displaying PS cell membrane proteins with DNA still confined within the cell. Cells in Q4 presented positive for Annexin V-FITC and negative for PI.

Figure 4.4 demonstrates the averaged cellular distribution in the samples per quadrant. The cell population percentages from the statistical data were averaged from the three samples per treatment. The analysed data is listed in figure A2 in the appendix. The Q1 data point showing 0,0% total cell population across all the samples was removed from figure 4.4, as this implies that the cell membranes were not completely impaired.

The data indicates a generally adverse effect of ezetimibe in promoting cellular apoptosis in human lung cancer cells. The most considerably affected samples were treated with concentrations of 20 µM ezetimibe, while samples treated with 40 µM ezetimibe concentrations recorded a small percentage of cells in stages of apoptosis. The apoptosis analysis also demonstrated that the ethanol vehicle promoted some apoptotic activity in the A549 cell line, indicating a slight cytotoxic effect caused by the ethanol vehicle. The highest concentration value of ezetimibe, 60 µM, indicated no influence over the A549 cells. While some samples showed to promote cellular apoptosis, no statistical significance was seen between any of the treated compared to the untreated samples.

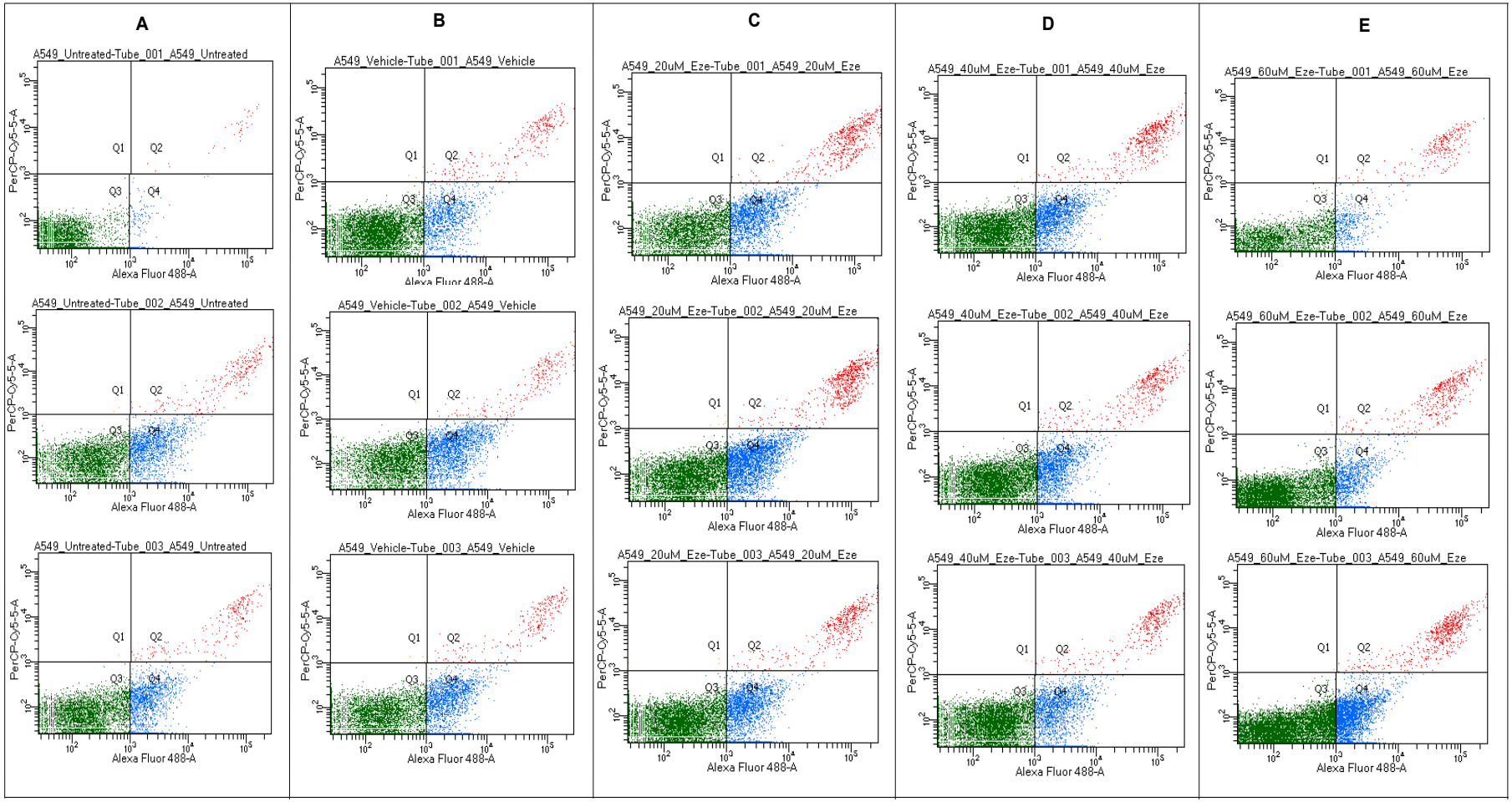

Figure 4. 3: A549 treated with ezetimibe in stages of apoptosis. The A549 cells are populated in stages of apoptosis based on the detection of fluorescent dyes Annexin V-FITC represented as Alexa Fluor 488-A and PI, represented as PerCP-Cy5-5-A. Cells in Q1 were completely impaired, cells in Q2 were in late-stage apoptosis, Q3 represents live cells and cells in Q4 were in early-stage apoptosis. Three biological replicates were conducted within the experiment, represented in each panel. **A**: untreated samples; **B**: ethanol vehicle; **C**: 20 µM ezetimibe; **D**: 40 µM ezetimibe; **E**: 60 µM ezetimibe. Cellular apoptosis indicated in Q2 and Q4, is mostly promoted at 20 µM ezetimibe concentrations, with some apoptotic activity seen in 40 µM and the ethanol vehicle. Ezetimibe seems ineffective in inducing apoptosis at 60 µM concentrations.

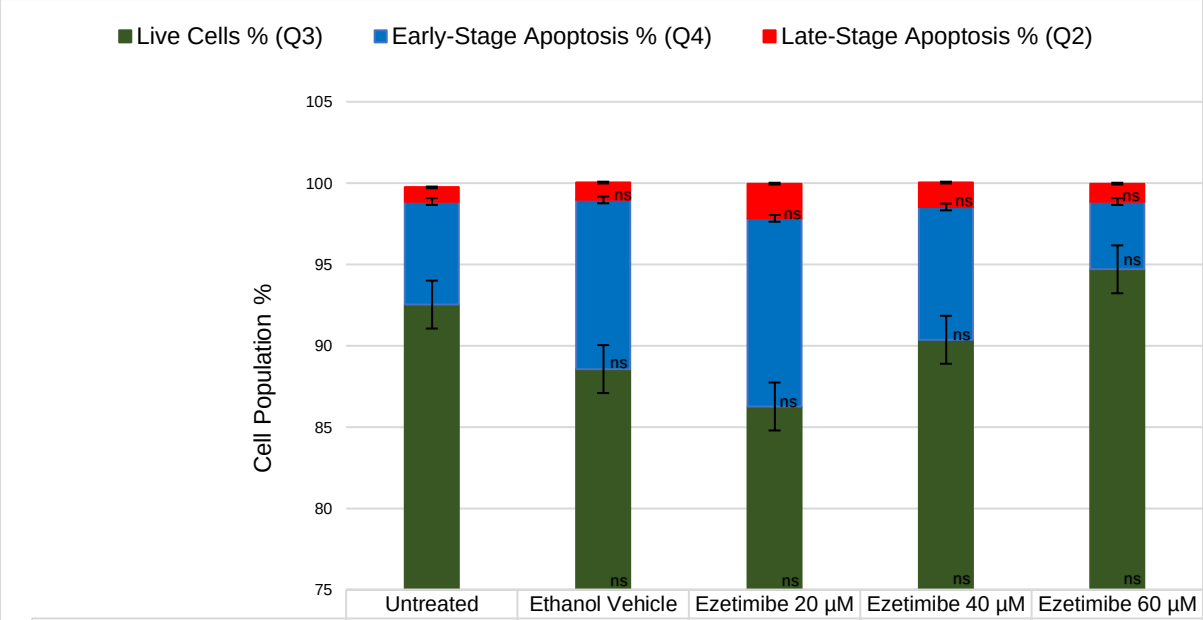

	Untreated	Ethanol Vehicle	Ezetimibe 20 µM	Ezetimibe 40 µM	Ezetimibe 60 µM
Late-Stage Apoptosis % (Q2)	1	1	2	2	1
Early-Stage Apoptosis % (Q4)	6	10	12	8	4
Live Cells % (Q3)	93	89	86	90	95

Figure 4. 4: **Percentage of A549 cells treated with ezetimibe in stages of apoptosis.** The averaged statistical data was calculated from the three samples of the apoptosis analysis in figure 4.3. The A549 cells are distributed into live cells, early-stage apoptosis cells and cells in late-stage apoptosis or necrosis. Apoptosis is mostly promoted at the 20 µM ezetimibe concertation, with some apoptotic activity seen at 40 µM and in the ethanol vehicle. Ezetimibe proved ineffective in promoting apoptosis at 60 µM. The experimental data compared untreated A549 cells to each concentration of the treated A549 cells. The data were considered statistically significant when the p-value was ≤ 0.05. The $p \leq 0.0001$ (****), $p \leq 0.001$ (***) and $p \leq 0.01$ (**) values were considered statistically significant, while $p \geq 0.05$ was not considered statistically significant (ns).

4.2.2 Cell cycle analysis

The stages of the cell cycle are represented by the DNA content in the cells. When not actively in the process of cell replication, cells have two copies of each chromosome (2N). The 2N stage can represent two cell cycle phases, namely the G1 phase, where the cells are not presently replicating but retain the ability to replicate, or the G0 phase when cellular senescence occurs. When cells are in the process of active replication, the DNA within the cells are copied and is between 2N and 4N. The DNA content ranging from 2N to 4N represents the S phase of the cell cycle. When DNA synthesis is complete, cells have four copies of each chromosome (4N), as the DNA content has doubled. The 4N stage can also represent two cell cycle phases, namely the G2 phase, where the cells are in a state of rest, or the M phase when cellular mitosis occurs. Typically, the flow cytometry histogram of healthy

untreated cells displays most of the cells in the G0/G1 phase of the cell cycle (2N), with some cells in the S phase undergoing DNA synthesis (2N - 4N) and the remainder of the population in the G2/M phase (4N). Only a few cells are apoptotic (< 2N) or have an excess of 4N DNA content (> 4N).

Figure 4.5 shows the cell cycle analysis of A549 cells treated with ezetimibe concentrations that were introduced to the PI fluorescent. Most of the samples show an initial peak on the x-axis of the histogram between 0 - 10^2 indicating chromosomal DNA in the G1 phase. The peak ranging between 10^3 - 10^4 indicates chromosomal DNA in the S phase and the 10^4 peak indicates DNA in the G2 phase. The histograms show the untreated sample (A) tube 1 and the 60 µM ezetimibe concentration sample (E) tube 3 as clear outliers, and with no statistical data recorded for these samples, they were discounted during data review.

The histograms in figure 4.5 were overlayed per treatment in figure A3 in the appendix. This shows the similar peak positions within each sample group, with variations in the cell count. The statistical data from figure 4.5 was summarised in figure 4.6. The raw data points are presented in table A1 in the appendix. Supplementary information includes the <G1 cell population which indicates apoptotic cells with a DNA content of < 2N and the >G2 cell population with an excess DNA content of > 4N.

It should be noted that the statistical data points in figure 4.6 were calculated by the FlowJo software based on the cell cycle results. The Dean-Jett-Fox model was applied to quantify the percentage of the cell population in the distinct cell cycle phases (Fox, 1980). This statistical model fits a second-order polynomial to the S phase. This modification allows for negative values and percentages over a hundred, as the calculations were based on S phase distribution, and not whole-sample distribution.

The data indicate a generally adverse effect of ezetimibe in the cell cycle process of human lung cancer cells. The 20 µM ezetimibe concentration showed to affect A549 with statistical significance, while 40 µM ezetimibe concentrations showed a small percentage of cells in stages different to the untreated samples. The cell cycle analysis also demonstrated that the ethanol vehicle statistically significantly promotes some cell cycle activity in the A549. The 60 µM ezetimibe concentration indicated no influence over the A549 cells.

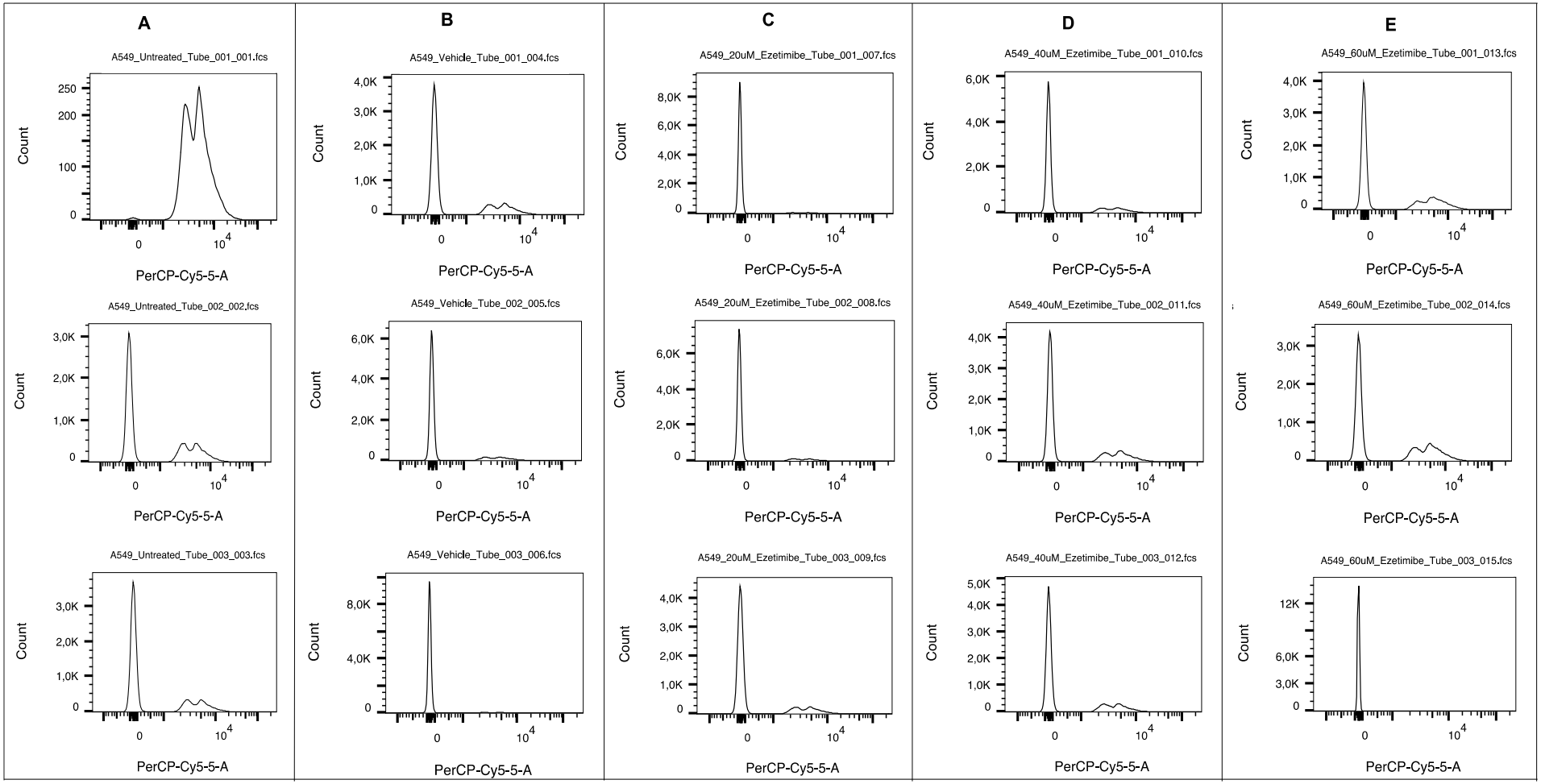

Figure 4. 5: Cell cycle analysis of A549 treated with ezetimibe. The histograms of cell cycle analysis on A549 cells treated with ezetimibe are shown. The cell count indicates the number of cells treated with PI, represented as PerCP-Cy5-5-A. Three biological replicates were conducted within the experiment, represented in each panel. **A**: untreated; **B**: ethanol vehicle; **C**: 20 µM ezetimibe; **D**: 40 µM ezetimibe; **E**: 60 µM ezetimibe. Changes in the cell cycle activity was observed at 20 µM and 40 µM ezetimibe concentrations. Ezetimibe seems ineffective in affecting the cell cycle at 60 µM concentration.

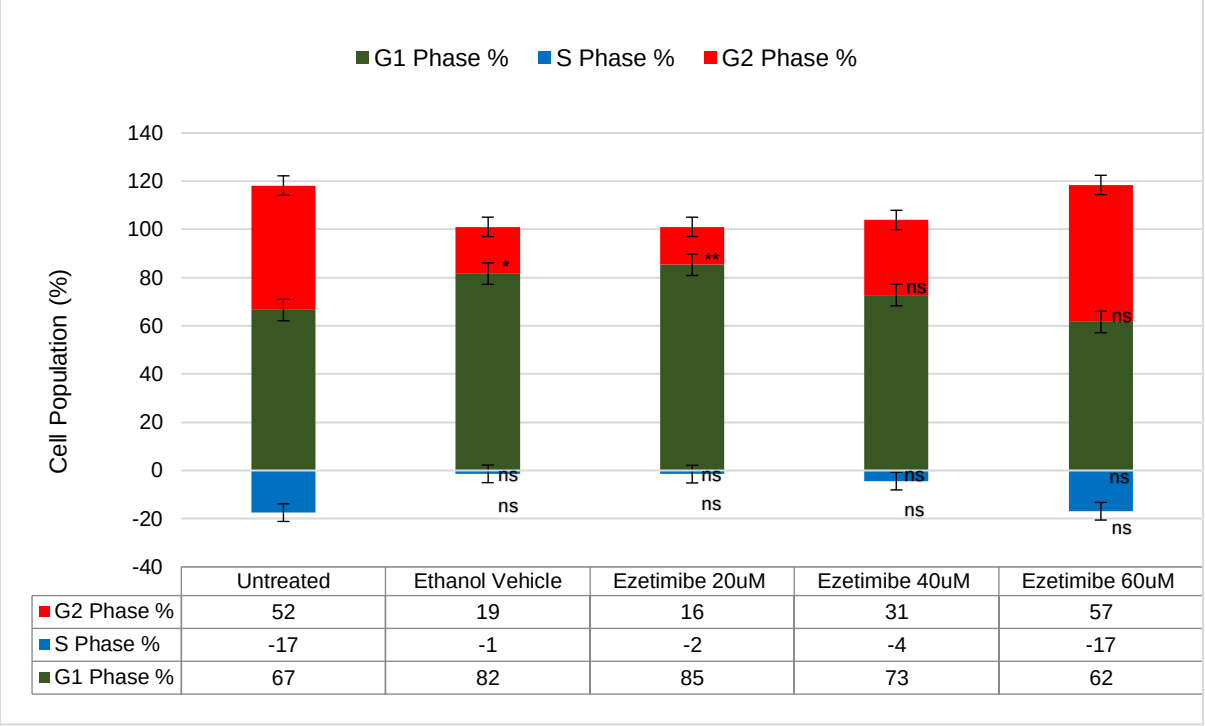

	Untreated	Ethanol Vehicle	Ezetimibe 20uM	Ezetimibe 40uM	Ezetimibe 60uM
G2 Phase %	52	19	16	31	57
S Phase %	-17	-1	-2	-4	-17
G1 Phase %	67	82	85	73	62

Figure 4. 6: Statistical data of A549 cells treated with ezetimibe during cell cycle analysis. The statistical data of the cell cycle analysis seen in figure 4.5 were averaged per treatment. Ezetimibe mainly promoted cell activity at 20 µM, with some activity seen at 40 µM and in the ethanol vehicle. Ezetimibe proved ineffective in promoting cell cycle activity at 60 µM. The complete data points are displayed in table A1 in the appendix as determined by the Dean-Jett-Fox model. The experimental data compared untreated A549 cells to the treated A549 cells. The data were considered statistically significant when the p-value was ≤ 0.05. The $p \leq 0.0001$ (****), $p \leq 0.001$ (***) and $p \leq 0.01$ (**) values were considered statistically significant, while $p \geq 0.05$ was not considered statistically significant (ns).

4.3 Molecular targets of ezetimibe

4.3.1 DARTS

The molecular targets of ezetimibe were identified through DARTS using A549 cells. The pronase stock solutions of 1:100, 1:300, 1:500, 1:1000 and, 1:3000 was made with the ethanol vehicle controls and the ezetimibe-treated samples. The cell lysates were loaded onto SDS-PAGE gels and the proteins in the samples were separated with electrophoresis according to size. This expected molecular weight of MDM2 is 55 kDa, however, the molecular target proteins of ezetimibe were protected from degradation, and thus clearly visible. The

undigested fragments were selected and cut from the SDS-PAGE gel for LC-MS protein analysis.

Figure 4.7 shows the SDS-PAGE gels. Pronase dilution 1:100 presented clear bands in the ezetimibe-treated sample proximate to the 50 kDa mark. These bands were visibly absent in the 1:100 vehicle-treated sample indicating proteasomal degradation. The visible bands were cut from the gel, as demonstrated in figure 4.7.

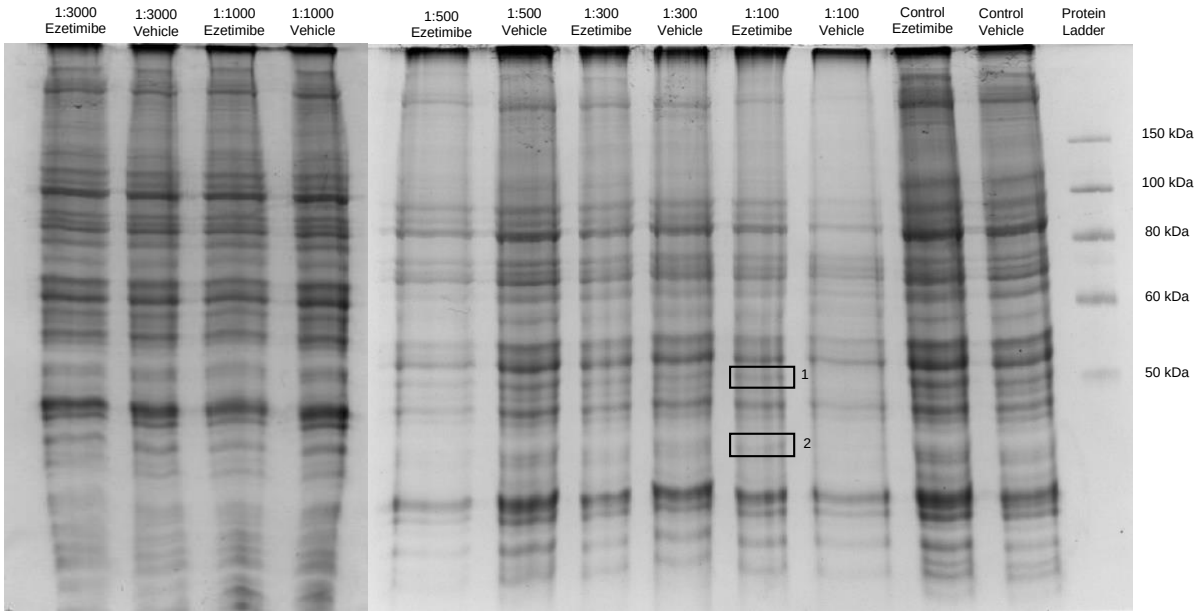

Figure 4. 7: DARTS SDS-PAGE gel. The proteins in A549 cells treated with ezetimibe, and degraded with protease dilutions 1:100, 1:300, 1:500, 1:1000 and 1:3000 is shown. Visualised by electrophoresis, the selected protein bands were certified. The 1:100 pronase dilution shows clear bands at the 50 kDa mark in the ezetimibe lane that is visibly absent in the vehicle lane.

The mass spectrometry identified the proteins in both samples taken from the SDS-PAGE gel. The molecular targets of ezetimibe were identified in the excised protein bands, however, the expected MDM2 protein was not listed in these results. The complete list of proteins that were identified by LC-MS can be found as a supporting document. Proteins of interest were selected based on a molecular weight from 45 – 55 kDa for sample 1 and below 50 kDa for sample 2. Additionally, the keratin-linked proteins and some housekeeping genes were removed. The proteins that were identified, and within these specifications, are listed in table 4.2. The complete list of mass spectrometry results was attached as a supplementary document. All the proteins that were identified were potential molecular targets of ezetimibe and could provide significant therapeutic potencies. These molecular targets have not been conclusively

validated in this study; however, future studies can be done to refine the investigation of these targeted molecules.

Table 4. 2: **Potential molecular targets of ezetimibe**

Sample 1			
Protein	**MW (kDa)**	**Location**	**Function**
DnaJ homolog subfamily A member 1	45	Cytoplasm	Stimulates ATP hydrolysis (Rauch & Gestwicki, 2014). Associated with protein transport into the mitochondria as co-chaperone. Negative regulator of BAX translocation from the cytosol to the mitochondria (Gotoh *et al*., 2004. It also promotes apoptosis in response to stress signals, as mediated by ultraviolet exposure (Stark *et al*., 2014).
Septin-7	45	Nucleus	Centrosome protein that certifies microtubule nucleation and S phase entry (Kuo *et al*., 2015).
Eukaryotic initiation factor 4A-I	46	Cytosol	ATP-dependant RNA helicases are associated with protein translation by unwinding the RNA secondary structure within the 5'-UTR of mRNA and recruiting the 43S pre-initiation complex (Loh *et al*., 2009).
Heterogeneous nuclear ribonucleoprotein F	46	Nucleus	Component of the heterogeneous nuclear ribonucleoprotein complexes associated with pre-mRNAs processing. Regulates alternative splicing. Binds pre-mRNAs sequences that are guanine-rich and stabilizes unfolded target RNA (Dominguez *et al*., 2010).
Adenosylhomocysteinase	48	Cytoplasm	Converts S-adenosylhomocysteine to adenosine and homocysteine (Yin *et al*., 2000).
Alpha-enolase	48	Cytoplasm	Glycolytic enzyme functions as a DNA binding protein and a plasminogen receptor (Huang *et al*., 2018; Sugahara *et al*., 1992), and also plays an important role in cancer development (Ghosh *et al*., 1999).
Protein disulfide-isomerase A6	48	ER	Chaperone inhibiting the aggregation of misfolded proteins (Kikuchi *et al*., 2002). Negatively regulates the unfolded protein response (UPR) by binding UPR sensors (Eletto *et al*., 2014).
Eukaryotic peptide chain release factor subunit 1	49	Cytoplasm	In response to termination codons UAG, UGA, and UAA, this protein directs the termination of nascent peptide translation (Feng *et al*., 2014; Flolova *et al*., 1994).
Aldehyde dehydrogenase, dimeric NADP-preferring	50	Cytoplasm	Detoxifies alcohol-derived acetaldehyde and mediates the metabolism of corticosteroids, lipid peroxidation, neurotransmitters, and biogenic amines (Hsu *et al*., 1992).
Putative elongation factor 1-alpha-like 3	50	Cytoplasm	Promotes the binding of aminoacyl-tRNA to the ribosomal A-site via GTP (Becker *et al*., 2013; Hamrita *et al*., 2011).
RuvB-like 1	50	Cytoplasm	Displays ATP-dependent DNA helicase (3' to 5') and single-stranded DNA-stimulated ATPase activity. Forms a hexamer that may be critical for ATP hydrolysis (Puri *et al*., 2007). Also, functions related to transcription factors include cell cycle regulation and, cancer development (Wood *et al*., 2000).
Peptidyl-prolyl cis-trans isomerase FKBP4	52	Cytoplasm	Immunophilin protein with co-chaperone functions. Interacts with heat-shock protein 90 (HSP90) to form steroid receptors heterocomplexes (Peattie *et al*., 1992). Possible intracellular trafficker of steroid hormone receptors between the cytoplasm and nuclear sectors (Sanchez *et al*., 1990). It also promotes microtubule assembly and may assist with mitochondrial oxidative stress (Gallo *et al*., 2011).
Bleomycin hydrolase	53	Cytoplasm	While the main physiological role of this protein is unknown, it does catalyse the antitumor drug BLM via hydrolases, which protects both normal and malignant cells from BLM toxicity (Chen *et al*., 2012).

Cytosolic non-specific dipeptidase	53	Cytoplasm	Catalyses the peptide bond in dipeptide proteins via hydrolysis. Mediator of the threonyl dipeptide catabolism (Kaur *et al*., 2009; Teufel *et al*., 2003). Catalyses N-lactoyl-amino acids to generate lactic acid and amino acids via hydrolysis and proteolysis (Jansen *et al*., 2015). Regulates apoptosis and cell cycle arrest (Zhang *et al*., 2006; Zhang *et al*., 2014).
Epoxide hydrolase 1	53	ER	Activates and detoxifies polycyclic aromatic hydrocarbons and assist in endogenous lipid metabolism such as fatty acids containing epoxide (Decker *et al*., 2012).
Rab GDP dissociation inhibitor beta	53	Cytoplasm	Prevents the exchange of GDP to GTP for most Rab proteins. This keeps GTPases inactively bound to GDP, regulating intracellular membrane trafficking (Zhang *et al*., 2015).
Aldehyde dehydrogenase family 3 member A2	55	Microsome	Remove toxic aldehydes generated by lipid peroxidation and the metabolism of alcohol. Catalyses the oxidation of both saturated and unsaturated aliphatic long-chain aldehydes into fatty acids (Kelson *et al*., 1997; Sanders *et al*., 2008).
		Sample 2	
Heterogeneous nuclear ribonucleoprotein A3	38	Nucleus	Participates in transporting RNA in the cytoplasm. Possibly assists in pre-mRNA splicing (Ma *et al*., 2002).
Nuclear migration protein nudC	38	Cytoplasm and nucleus	Participates in neuronal migration and neurogenesis. Assists in chromosome separation and mitotic spindle formation during mitosis (Chen *et al*., 2015). Also essential for cell proliferation and cytokinesis (Aumais *et al*., 2003).
SUMO-activating enzyme subunit 1	38	Nucleus	Heterodimer acting as an E1 ligase for SUMO1, SUMO2, SUMO3, and SUMO4. Also mediates ATP-dependent SUMO activation (Desterro *et al*., 1999; Tatham *et al*., 2001).
Serine-threonine kinase receptor-associated protein	39	Cytoplasm and nucleus	Catalyses the assembly of small nuclear ribonucleoproteins assembly, required for pre-mRNA splicing (Chari *et al*., 2008).
Casein kinase II subunit alpha 3	41	Cytosol	Catalyses the phosphorylation of serine or threonine in C-terminal acidic residues as a subunit of the serine/threonine-protein kinase complex. Acts as a amplification-dependent oncogene by promoting tumorigenesis and cell proliferation through the down-regulation of the tumor suppressor protein, PML. Possibly involved in the pathogenic development and progression of lung cancer (Hung *et al*., 2010).
Guanine nucleotide-binding protein subunit alpha-13	44	Cytoplasm and melanosome	Modulates numerous transmembrane signaling systems. Also activates the RhoA/ROCK signaling pathway which promotes metastasis and the invasion of tumor cells (Kelly *et al*., 2006).
Transmembrane protein 43	45	Nucleus and ER	Maintains the structure of the nuclear envelope through protein organization. Also modulates innate immune signaling (Jiang *et al*., 2017).
Aspartate aminotransferase, mitochondrial	48	Mitochondria	Catalyses the transamination of the L-tryptophan metabolite to form kynurenic acid (van Karnebeek *et al*., 2019). Essential in intracellular NAD(H) redox balance. Assists in amino acid metabolic exchange between the cytosol and mitochondria (Zhou *et al*., 1998).
Eukaryotic translation initiation factor 3 subunit H	50	Cytoplasm	Component of the eukaryotic translation initiation factor 3 complex, involved in protein synthesis. By initiating the translation of mRNAs, this protein assists in cell proliferation, cell cycle, cellular differentiation and apoptosis, and translational activation or repression. This complex also stimulates mRNA recruitment and scans mRNA agents for AUG recognition. It also assists with the disassembly and recycling of ribosomal complexes (Lee *et al*., 2015; Masutani *et al*., 2007).

Chapter 5: Discussion

5.1 Ezetimibe is toxic in A549 cells

Ezetimibe was tested in human embryonic kidney cells (HEK293), human breast cancer cells (MCF-7), and human lung cancer cells (A549). The results showed that ezetimibe does not influence the growth of HEK293 of MCF-7 cells, irrespective of the ezetimibe concentrations administered. This non-toxic effect of ezetimibe on HEK293 cells could be due to the distinctly low levels of p53 recorded in normal cells. As the negative regulator of p53, MDM2 levels would be correspondingly low. MDM2 is a potential molecular target of ezetimibe, however, in cells with low MDM2 levels, ezetimibe would be ineffectual.

The cytotoxicity of ezetimibe in A549 cells, however, was profound. Ezetimibe proved highly toxic to human lung cancer cells, killing half of the cell population at a concentration of 48 µM. Ezetimibe, however, proved non-toxic in MCF-7 cells, which is also a cancerous cell line. Variations in the expression of p53 between these cell lines could explain this outcome. Both A549 and MCF-7 cells express wild-type p53, however, MCF-7 cells are known to overexpress MDM2 (Saji *et al*., 1999). The increased concentrations of MDM2 could reduce the efficacy of ezetimibe and explain the consistent cellular growth of these cells when treated with the drug.

Ezetimibe is primarily designed to inhibit low-density lipoprotein cholesterol (LDL-C). While this activity of ezetimibe proves critical in the small intestine, it is negated in the absence of the cholesterol absorption mediator, the Niemann-Pick C1-like 1 (NPC1L1) protein. The NPC1L1 protein is selectively located in the gastrointestinal tract at the brush border of jejunal enterocytes (Altmann *et al*., 2004; Bays, 2002; Davis *et al*., 2011; Rosenblum *et al*., 1998). The cholesterol lowering abilities associated with ezetimibe are thus only active through oral ingestion and would not influence the drug treated cell cultures.

5.2 Ezetimibe is limited in affecting apoptosis and cell cycle activity in A549 cells

Ezetimibe was expected to induce apoptosis and cell cycle arrest in A549 cells, based on the reduced cell population reported in the MTT assay of this cell line. The elevated p53 levels, mediated by ezetimibe, would potentially activate downstream genes associated with cell cycle arrest (p21 and GADD45) and apoptosis (PUMA, BAX and NOXA). However, ezetimibe

proved limited in the ability to induce apoptosis and/or cell cycle arrest in the human lung cancer cell line. Apoptosis was seen in the 20 µM ezetimibe concentrations, while no apoptosis was induced in the 40 µM and 60 µM concentrations. While cellular apoptotic death was observed, the activity had no statistical significance when comparing the treated to the untreated samples.

Similarly, the effect of ezetimibe on the cell cycle phases of A549 was minimal, with cell cycle activity seen in 20 µM and 40 µM concentrations. The slight changes to the cell cycle were consistent with the checkpoints regulated by p53. Cells at the G1/S phase checkpoint are monitored by p53 before DNA replication. The peaks in the G1-phase of 20 µM and 40 µM concentrations suggest that these cells were not replicating or in cellular senescence. Additionally, p53 monitors cells at the G2/M phase checkpoint before mitosis. The low cell count in the S and G2 phase peaks suggests that fewer cells (20 µM and 40 µM) were undergoing DNA synthesis, were in a state of rest or were undergoing cellular mitosis. While the effect of ezetimibe on the cell cycle was moderate, the presence of ezetimibe did induce some cell cycle activity corresponding to p53 functions.

The ethanol vehicle promoted some apoptotic and cell cycle activity in the A549 cell line. These findings are in contradiction with the MTT assay, which showed that ethanol was not toxic in A549 cells. Additionally, the highest concentration of ethanol (0.6%) utilized in the flow cytometry samples should not promote cytotoxicity. Ethanol concentrations lower than 1.25% do not induce significant cytotoxic alterations in A549 cells when diluted in media (Khare *et al*., 2022; Nguyen et al., 2020). The reported toxicity of the ethanol vehicle and the contradictions in the flow cytometry data compared to the MTT assay warrants the repetition of these methods. The limited cellular changes caused by ezetimibe in apoptosis and cell cycle analysis (particularly at high concentrations) also support experimental repeats in the future.

5.3 Therapeutical significance of the molecular targets of ezetimibe

While the computational model revealed high-affinity binding between ezetimibe and MDM2, results from the DARTS experiments revealed no definite complex formed between these molecules. The limitations of DARTS include inaccurate sampling or LC-MS sensitivity during detection. Additionally, the MDM2 expression in these samples could have been insufficient or the molecular affinity was inadequate. The molecular targets of ezetimibe that were,

however, identified by DARTS, could provide insight into potential molecular targets of ezetimibe. These proteins could have significant therapeutic capability based on their affinity to ezetimibe, unlimited to oncogenesis. The results from the DARTS could serve as a preliminary study for future work.

5.4 The oncological potential of ezetimibe

The cytotoxic effect and molecular changes mediated by ezetimibe in human lung cancer cells were significant. When these findings are combined with being non-toxic to human embryonic kidney cells, ezetimibe presents as a plausible therapeutical agent for lung cancer. The impact of ezetimibe could prospectively be increased in combination with other agents, or ezetimibe could serve as a scaffold for further drug design. Regardless of the application, ezetimibe indicates strong oncological potential.

Chapter 6: Conclusion

This project aimed to determine the cytotoxicity and molecular targets of ezetimibe in cancerous cells. The toxic effects of ezetimibe in both normal and cancer cell lines were tested to investigate ezetimibe as a possible anti-cancer agent. Ezetimibe proved toxic to the lung cancer cell line and not toxic to the normal cell line and breast cancer cell line at the same concentrations. The regulatory mechanisms of ezetimibe were shown to be limited in the cellular characteristics of apoptotic cancerous cells and the cell cycle analysis of cancerous cells. Ezetimibe perturbs the cell cycle and induces apoptosis by a currently unknown mechanism. The molecular targets of ezetimibe in cancerous cells were identified and deduced to have significant therapeutic potential in combination with ezetimibe. Multiple potential targets were identified though DARTS, but no target could be confirmed, with MDM2 not detected. Ezetimibe was found to influence the toxicology and cellular mechanisms of lung cancer cells. This substantiates the use of ezetimibe as an effective potential anti-cancer therapeutic for human lung cancer, as it targets and kills human lung cancer cells without affecting normal healthy cells.

References

Altmann, S.W., Davis, H.R. Jr., Zhu, L.J., Yao, X., Hoos, L.M., Tetzloff, G., Iyer, S.P., Maguire, M., Golovko, A., Zeng, M., Wang, L., Murgolo, N. & Graziano, M.P. 2004. Niemann-Pick C1 Like 1 protein is critical for intestinal cholesterol absorption. *Science,* 303(5661):1201-1204.

Argentini, M., Barboule, N. & Wasylyk, B. 2001. The contribution of the acidic domain of MDM2 to p53 and MDM2 stability. *Oncogene*, 20(11):1267-1275.

Aumais, J.P., Williams, S.N., Luo, W., Nishino, M., Caldwell, K.A., Caldwell, G.A., Lin, S.H. & Yu-Lee, L.Y. 2003. Role for NudC, a dynein-associated nuclear movement protein, in mitosis and cytokinesis. *Journal of cell science*, 116(10):1991-2003.

Baker, S.J., Fearon, E.R., Nigro, J.M., Hamilton, S.R., Preisinger, A.C., Jessup, J.M., van Tuinen, P., Ledbetter, D.H., Barker, D.F., Nakamura, Y., White, R. & Vogelstein, B. 1989. Chromosome 17 deletions and p53 gene mutations in colorectal carcinomas. *Science*, 244(4901):217-221.

Banin, S., Moyal, L., Shieh, S., Taya, Y., Anderson, C.W., Chessa, L., Smorodinsky, N.I., Prives, C., Reiss, Y., Shiloh, Y. & Ziv, Y. 1998. Enhanced phosphorylation of p53 by ATM in response to DNA damage. *Science,* 281(5383):1674-1677.

Bates, S. & Vousden, K.H. 1996. p53 in signalling checkpoint arrest or apoptosis. *Current Opinion in Genetics & Development,* 6(1):12-18.

Bays, H. 2002. Ezetimibe. *Expert Opinion on Investigational Drugs,* 11(11):1587-1604.

BD Biosciences. 2012. BD FACSAria™ III User's Guide. 23-11654-01 Rev. 01. Becton, Dickinson and Company.

Becker, M., Kuhse, J. & Kirsch, J. 2013. "Effects of two elongation factor 1A isoforms on the formation of gephyrin clusters at inhibitory synapses in hippocampal neurons". *Histochemistry and Cell Biology*, 140(6):603-609.

Beckerman, R. & Prives, C. 2010. Transcriptional regulation by p53. *Cold Spring Harbor perspectives in biology*, 2(8):a000935.

Bedford, L., Paine, S., Sheppard, P.W., Mayer, R.J. & Roelofs, J. 2010. Assembly, structure, and function of the 26S proteasome. *Trends in Cell Biol*ogy, 20(7):391-401.

Bodner, S.M., Minna, J.D., Jensen, S.M., D'Amico, D., Carbone, D., Mitsudomi, T., Fedorko, J., Buchhagen, D.L., Nau, M.M,, Gazdar. A.F, *et al*. 1992. Expression of mutant p53 proteins in lung cancer correlates with the class of p53 gene mutation. *Oncogene,* 7(4):743-749.

Bousquet-Dubouch, M.P., Fabre, B., Monsarrat, B. & Burlet-Schiltz, O. 2011. Proteomics to study the diversity and dynamics of proteasome complexes: from fundamentals to the clinic. *Expert Review of Proteomics*, 8(4):459-481.

Brugarolas, J., Chandrasekaran, C., Gordon, J.I., Beach, D., Jacks, T. & Hannon, G.J. 1995. Radiation-induced cell cycle arrest compromised by p21 deficiency. *Nature,* 377(6549):552-527.

Canman, C.E., Lim, D.S., Cimprich, K.A., Taya, Y., Tamai, K., Sakaguchi, K., Appella, E., Kastan, M.B. & Siliciano, J.D. 1998. Activation of the ATM kinase by ionizing radiation and phosphorylation of p53. *Science,* 281(5383):1677-1679.

Carr, M.I. & Jones, S.N. 2016. Regulation of the MDM2-p53 signalling axis in the DNA damage response and tumorigenesis. *Translational Cancer Research,* 5(6):707-724.

Catapano, A.L. 2009. Perspectives on low-density lipoprotein cholesterol goal achievement. Current medical research and opinion, 25(2):431-447.

Chansky, K., Detterbeck, F.C., Nicholson, A.G., Rusch, V.W., Vallières, E., Groome, P., Kennedy, C., Krasnik, M., Peake, M., Shemanski, L., Bolejack, V., Crowley, J.J., Asamura, H., Rami-Porta, R. & IASLC Staging and Prognostic Factors Committee, Advisory Boards, and Participating Institutions. 2017. The IASLC Lung Cancer Staging Project: External Validation of the Revision of the TNM Stage Groupings in the Eighth Edition of the TNM Classification of Lung Cancer. *Journal of thoracic oncology: official publication of the International Association for the Study of Lung Cancer*, 12(7):1109-1121.

Chao, C., Hergenhahn, M., Kaeser, M.D., Wu, Z., Saito, S., Iggo, R., Hollstein, M., Appella, E. & Xu, Y. 2003. Cell type- and promoter-specific roles of Ser18 phosphorylation in regulating p53 responses. *The Journal of biological chemistry*, 278(42):41028-41033.

Chari, A., Golas, M.M., Klingenhäger, M., Neuenkirchen, N., Sander, B., Englbrecht, C., Sickmann, A., Stark, H. & Fischer, U. 2008. An assembly chaperone collaborates with the SMN complex to generate spliceosomal SnRNPs. *Cell*, 135(3):497-509.

Chehab, N.H., Malikzay, A., Stavridi, E.S. & Halazonetis, T.D. 1999. Phosphorylation of Ser-20 mediates stabilization of human p53 in response to DNA damage. *Proceedings of the Natural Academy of Science of the United States of America*, 96(24):13777-13782.

Chen, C.Y., Oliner, J.D., Zhan, Q., Fornace Jr, A.J., Vogelstein, B. & Kastan, M.B. 1994. Interactions between p53 and MDM2 in a mammalian cell cycle checkpoint pathway. *Proceedings of the Natural Academy of Science of the United States of America*, 91(7):2684-2688.

Chen, D., Ito, S., Yuan, H., Hyodo, T., Kadomatsu, K., Hamaguchi, M. & Senga, T. 2015. EML4 promotes the loading of NUDC to the spindle for mitotic progression. *Cell cycle (Georgetown, Tex.)*, 14(10):1529-1539.

Chen, J., Chen, Y. & He, Q. 2012. Action of bleomycin is affected by bleomycin hydrolase but not by caveolin-1. *International journal of oncology*, 41(6):2245-2252.

Chen, J., Marechal, V. & Levine, A.J. 1993. Mapping of the p53 and mdm-2 interaction domains. *Molecular and cellular biology,* 13(7):4107-4114.

Chen, J., Wu, X., Lin, J. & Levine, A.J. 1996. Mdm-2 inhibits the G1 arrest and apoptosis functions of the p53 tumor suppressor protein. *Molecular and cellular biology,* 16(5):2445-2452.

Chen, T., Ozel, D., Qiao, Y., Harbinski, F., Chen, L., Denoyelle, S., He, X., Zvereva, N., Supko, J.G., Chorev, M., Halperin, J.A. & Aktas, B.H. 2011. Chemical genetics identify eIF2alpha kinase heme-regulated inhibitor as an anticancer target. *Nature chemical biology,* 7(9):610-616.

Chen, Z., Trotman, L.C., Shaffer, D., Lin, H.K., Dotan, Z.A., Niki, M., Koutcher, J.A., Scher, H.I., Ludwig, T., Gerald, W., Cordon-Cardo, C. & Pandolfi, P.P. 2005. Crucial role of p53-dependent cellular senescence in suppression of Pten-deficient tumorigenesis. *Nature*, 436(7051):725-730.

Chibi, M., Meyer, M., Skepu, A., Rees, D.J.G., Moolman-Smook, J.C., & Pugh, D.J.R. 2008. RBBP6 Interacts with Multifunctional Protein YB-1 through Its RING Finger Domain, Leading to Ubiquitination and Proteasomal Degradation of YB-1. *Journal of Molecular Biology,* 384(4):908-916.

Choi, J. & Donehower, L.A. 1999. p53 in embryonic development: maintaining a fine balance. *Cellular and Molecular Life Sciences,* 55:38-47.

Ciccia, A. & Elledge, S.J. 2010. The DNA damage response: making it safe to play with knives. *Molecular Cell,* 40(2):179-204.

Clark, A.R., Purdie, C.A., Harrison, D.J., Morris, R.G., Bird, C.C., Hooper, M.L. & Wyllie, A.H. 1993. Thymocyte apoptosis induced by p53-dependent and independent pathways. *Nature,* 362(6423):849-852.

Climent, E., Marco-Benedí, V., Benaiges, D., Pintó, X., Suárez-Tembra, M., Plana, N., Lafuente, H., Ortega-Martínez de Victoria, E., Brea-Hernando, A., Vila, A., Civeira, F. & Pedro-Botet, J. 2021. Impact of statin therapy on LDL and non-HDL cholesterol levels in subjects with heterozygous familial hypercholesterolaemia. *Nutrition, Metabolism and Cardiovascular Diseases,* DOI: 10.1016/j.numecd.2021.01.014 Reviewed 04/02/2020.

Cordon-Cardo, C., Latres, E., Drobnjak, M., Oliva, M.R., Pollack, D., Woodruff, J.M., Marechal, V., Chen, J., Brennan, M.F. & Levine, A.J. 1994. Molecular abnormalities of mdm2 and p53 genes in adult soft tissue sarcomas. *Cancer research,* 54(3):794-799.

Davis, H.R. Jr., Tershakovec, A.M., Tomassini, J.E. & Musliner, T. 2011. Intestinal sterol transporters and cholesterol absorption inhibition. *Current Opinion in Lipidology,* 22(6):467-478.

Decker, M., Adamska, M., Cronin, A., Di Giallonardo, F., Burgener, J., Marowsky, A., Falck, J.R., Morisseau, C., Hammock, B.D., Gruzdev, A., Zeldin, D.C. & Arand, M. 2012. EH3 (ABHD9): the first member of a new epoxide hydrolase family with high activity for fatty acid epoxides. *Journal of lipid research*, 53(10):2038-2045.

DeLeo, A.B., Jay, G., Appella, E., Dubois, G.C., Law, L.W. & Old, L.J. 1979. Detection of a transformation-related antigen in chemically induced sarcomas and other transformed cells of the mouse. *Proceedings of the Natural Academy of Science of the United States of America*, 76(5):2420-2424.

Deng, C., Zhang, P., Harper, J.W., Elledge, S.J. & Leder, P. 1995. Mice lacking p21CIP1/WAF1 undergo normal development, but are defective in G1 checkpoint control. *Cell,* 82(4):675-684.

Desterro, J.M., Rodriguez, M.S., Kemp, G.D. & Hay, R.T. 1999. Identification of the enzyme required for activation of the small ubiquitin-like protein SUMO-1. *The Journal of biological chemistry*, 274(15):10618-10624.

de Toledo, S.M., Azzam, E.I., Dahlberg, W.K., Gooding, T.B. & Little, J.B. 2000. ATM complexes with HDM2 and promotes its rapid phosphorylation in a p53-independent manner in normal and tumor human cells exposed to ionizing radiation. *Oncogene,* 19(54):6185-6193.

Dominguez, C., Fisette, J.F., Chabot, B. & Allain, F.H. 2010. Structural basis of G-tract recognition and encaging by hnRNP F quasi-RRMs. *Nature structural & molecular biology*, 17(7):853-861.

Dumaz, N., Milne, D.M. & Meek, D.W. 1999. Protein kinase CK1 is a p53-threonine 18 kinase which requires prior phosphorylation of serine 15. *FEBS Letters,* 463(3):312-316.

el-Deiry, W.S., Tokino, T., Velculescu, V.E., Levy, D.B., Parsons, R., Trent, J.M., Lin, D., Mercer, W.E., Kinzler, K.W. & Vogelstein, B. 1993. WAF1, a potential mediator of p53 tumor suppression. *Cell,* 75(4):817-825.

Eletto, D., Eletto, D., Dersh, D., Gidalevitz, T. & Argon, Y. 2014. Protein disulfide isomerase A6 controls the decay of IRE1α signaling via disulfide-dependent association. *Molecular cell*, 53(4):562-576

Elmore, S. 2007. Apoptosis: A Review of Programmed Cell Death. *Toxicologic pathology*, 35(4):495-516.

Fakharzadeh, S.S., Trusko, S.P. & George, D.L. 1991. Tumorigenic potential associated with enhanced expression of a gene that is amplified in a mouse tumor cell line. *European Molecular Biology Organization Journal,* 10(6):1565-1569.

Fang, L., Igarashi, M., Leung, J., Sugrue, M.M., Lee, S.W. & Aaronson, S.A. 1999. p21Waf1/Cip1/Sdi1 induces permanent growth arrest with markers of replicative senescence in human tumor cells lacking functional p53. *Oncogene,* 18(18):2789-2797.

Fang, S., Jensen, J.P., Ludwig, R.L., Vousden, K.H. & Weissman, A.M. 2000. Mdm2 is a RING finger-dependent ubiquitin protein ligase for itself and p53. *Journal of Biological Chemistry*, 275(12):8945-8951.

Feng, T., Yamamoto, A., Wilkins, S.E., Sokolova, E., Yates, L.A., Münzel, M., Singh, P., Hopkinson, R.J., Fischer, R., Cockman, M.E., Shelley, J., Trudgian, D.C., Schödel, J., McCullagh, J.S., Ge, W., Kessler, B.M., Gilbert, R.J., Frolova, L.Y., Alkalaeva, E., Ratcliffe, P.J. & Coleman, M. L. 2014. Optimal translational termination requires C4 lysyl hydroxylation of eRF1. *Molecular cell*, 53(4):645-654.

Feng, Z. & Levine, A.J. 2010. The regulation of energy metabolism and the IGF-1/mTOR pathways by the p53 protein. *Trends in Cell Biology*, 20(7):427-434.

Finlay, C.A., Hinds, P.W. & Levine, A.J. 1989. The p53 proto-oncogene can act as a suppressor of transformation. *Cell*, 57(7):1083-1093.

Fox, M.H. 1980. A model for the computer analysis of synchronous DNA distributions obtained by flow cytometry. *Cytometry,* 1(1):71-77.

Franklin, W.A. 2000. Diagnosis of lung cancer: pathology of invasive and preinvasive neoplasia. *Chest*, 117(4):80S-89S.

Fridman, J.S. & Lowe, S.W. 2003. Control of apoptosis by p53. *Oncogene,* 22(56):9030-9040.

Frolova, L., Le Goff, X., Rasmussen, H.H., Cheperegin, S., Drugeon, G., Kress, M., Arman, I., Haenni, A.L., Celis, J.E., & Philippe, M. 1994. A highly conserved eukaryotic protein family possessing properties of polypeptide chain release factor. *Nature*, 372(6507):701-703.

Futamura, Y., Muroi, M. & Osada, H. 2013. Target identification of small molecules based on chemical biology approaches. *Molecular bioSystems*, 9(5):897-914.

Gallastegui, N. & Groll, M. 2010. The 26S proteasome: assembly and function of a destructive machine. *Trends in Biochemical Sciences,* 35(11):634-642.

Gallo, L.I., Lagadari, M., Piwien-Pilipuk, G. & Galigniana, M.D. 2011. The 90-kDa heat-shock protein (Hsp90)-binding immunophilin FKBP51 is a mitochondrial protein that translocates to the nucleus to protect cells against oxidative stress. *The Journal of biological chemistry*, 286(34):30152-30160.

Gama, V., Gomez, J.A., Mayo, L.D., Jackson, M.W., Danielpour, D., Song, K., Haas, A.L., Laughlin, M.J. & Matsuyama, S. 2009. Hdm2 is a ubiquitin ligase of Ku70-Akt promotes cell survival by inhibiting Hdm2-dependent Ku70 destabilization. *Cell Death Differentiation,* 16(5):758-769.

Gao, S., Witte, M.M. & Scott, R.E. 2002. P2P-R protein localizes to the nucleolus of interphase cells and the periphery of chromosomes in mitotic cells which show maximum P2P-R immunoreactivity. *Journal of Cellular Physiol*ogy, 191(2):145-154.

Ge, L., Wang, J., Qi, W., Miao, H.H., Cao, J., Qu, Y.X., Li, B.L. & Song, B.L. 2008. The cholesterol absorption inhibitor ezetimibe acts by blocking the sterol-induced internalization of NPC1L1. *Cell Metabolism,* 7(6):508-519.

Ghosh, A.K., Steele, R. & Ray, R.B. 1999. Functional domains of c-myc promoter binding protein 1 involved in transcriptional repression and cell growth regulation. *Molecular and cellular biology*, 19(4):2880-2886.

Goh, W.L., Lee, M.Y., Joseph, T.L., Quah, S.T., Brown, C.J., Verma, C., Brenner, S., Ghadessy, F.J. & Teo, Y.N. 2014. Molecular Rotors as Conditionally Fluorescent Labels for Rapid Detection of Biomolecular Interactions. *Journal of the American Chemical Society,* 136(17):6159-6162.

Gotoh, T., Terada, K., Oyadomari, S. & Mori, M. 2004. hsp70-DnaJ chaperone pair prevents nitric oxide- and CHOP-induced apoptosis by inhibiting translocation of Bax to mitochondria. *Cell death and differentiation*, 11(4):390-402.

Gu, J., Nie, L., Wiederschain, D. & Yuan, Z.M. 2001. Identification of p53 sequence elements that are required for MDM2-mediated nuclear export. *Molecular and cellular biology,* 21(24):8533-8546.

Hamrita, B., Nasr, H.B., Hammann, P., Kuhn, L., Guillier, C.L., Chaieb, A., Khairi, H. & Chahed, K. 2011. An elongation factor-like protein (EF-Tu) elicits a humoral response in infiltrating ductal breast carcinomas: an immunoproteomics investigation. *Clinical Biochemistry*, 44(13):1097-1104.

Harris, C.C. 1996. p53 tumor suppressor gene: from the basic research laboratory to the clinic--an abridged historical perspective. *Carcinogenesis*, 17(6):1187-1198.

Haupt, Y., Barak, Y. & Oren, M. 1996. Cell type-specific inhibition of p53-mediated apoptosis by mdm2. *European Molecular Biology Organization Journal,* 15(7):1596-1606.

Haupt, Y., Maya, R., Kazaz, A. & Oren, M. 1997. MDM2 promotes the rapid degradation of p53. *Nature*, 387(6630):296-299.

Hayashida, K., Daiba, A., Sakai, A., Tanaka, T., Kaji, K., Inaba, N., Ando, S., Najiyama, N., Terasaki, H., Abe, A., Ogasawara, M., Kohara, M., Harada, M., Okanoue, T., Ito, S. & Kaneko, S. 2005. Pretreatment prediction of interferon-alfa efficacy in chronic hepatitis C patients. *Clinical Gastroenterology and Hepatology,* 3(12):1253-1259.

Herbst, R.S., Morgensztern, D. & Boshoff, C. 2018. The biology and management of non-small cell lung cancer. *Nature,* 553:446-454.

Higashimoto, Y., Saito, S., Tong, X.H., Hong, A., Sakaguchi, K., Appella, E. & Anderson, C.W. 2000. Human p53 is phosphorylated on serines 6 and 9 in response to DNA damage-inducing agents. *The Journal of biological chemistry,* 275(30):23199-22303.

Hirao, A., Kong, Y.Y., Matsuoka, S., Wakeham, A., Ruland, J., Yoshida, H., Liu, D., Elledge, S.J. & Mak, T.W. 2000. DNA damage-induced activation of p53 by the checkpoint kinase Chk2. *Science,* 287(5459):1824-1827.

Hollstein, M., Sidransky, D., Vogelstein, B. & Harris, CC. 1991. P53 mutations in human cancers. *Science,* 253(5015):49-53.

Homer, C., Knight, D.A., Hananeia, L., Sheard, P., Risk, J., Lasham, A., Royds, J.A. & Braithwaite, A.W. 2005. Y-box factor YB1 controls p53 apoptotic function. *Oncogene,* 24(56):8314-8325.

Honda, R., Tanaka, H. & Yasuda, H. 1997. Oncoprotein MDM2 is a ubiquitin ligase E3 for tumor suppressor p53. *FEBS letters,* 420(1):25-27.

Honda, R. & Yasuda, H. 1999. Association of p19(ARF) with Mdm2 inhibits ubiquitin ligase activity of Mdm2 for tumor suppressor p53. *European Molecular Biology Organization Journal*, 18(1):22-27.

Hsu, L.C., Chang, W.C., Shibuya, A. & Yoshida, A. 1992. Human stomach aldehyde dehydrogenase cDNA and genomic cloning, primary structure, and expression in Escherichia coli. *The Journal of biological chemistry*, 267(5):3030-3037.

Huang, H., Tang, S., Ji, M., Tang, Z., Shimada, M., Liu, X., Qi, S., Locasale, J.W., Roeder, R.G., Zhao, Y. & Li, X. 2018. p300-Mediated Lysine 2-Hydroxyisobutyrylation Regulates Glycolysis. *Molecular cell*, 70(4):663-678.

Hung, M.S., Lin, Y.C., Mao, J.H., Kim, I.J., Xu, Z., Yang, C.T., Jablons, D.M. & You, L. 2010. Functional polymorphism of the CK2alpha intronless gene plays oncogenic roles in lung cancer. *PloS one*, 5(7):e11418.

Itahana, K., Dimri, G. & Campisi, J. 2001. Regulation of cellular senescence by p53. *European Journal of Biochemistry,* 268(10):2784-2791.

Ito, A., Lai, C.H., Zhao, X., Saito, S., Hamilton, M.H., Appella, E. & Yao, T.P. 2001. p300/CBP-mediated p53 acetylation is commonly induced by p53-activating agents and inhibited by MDM2. *The EMBO journal,* 20(6):1331-1340.

Jackson, S.P. & Bartek, J. 2009. The DNA-damage response in human biology and disease. *Nature,* 461(7267):1071-1078.

Jansen, R.S., Addie, R., Merkx, R., Fish, A., Mahakena, S., Bleijerveld, O.B., Altelaar, M., IJlst, L., Wanders, R.J., Borst, P. & van de Wetering, K. 2015. N-lactoyl-amino acids are ubiquitous metabolites that originate from CNDP2-mediated reverse proteolysis of lactate and amino acids. *Proceedings of the National Academy of Sciences of the United States of America*, 112(21):6601-6606.

Jiang, C., Zhu, Y., Zhou, Z., Gumin, J., Bengtsson, L., Wu, W., Songyang, Z., Lang, F.F. & Lin, X. 2017. TMEM43/LUMA is a key signaling component mediating EGFR-induced NF-κB activation and tumor progression. *Oncogene*, 36(20):2813-2823.

Kastan, M.B. & Lim, D.S. 2000. The many substrates and functions of ATM. *Nature Review Molecular Cell Biology,* 1(3):179-186.

Kaur, H., Kumar, C., Junot, C., Toledano, M.B. & Bachhawat, A.K. 2009. Dug1p Is a Cys-Gly peptidase of the gamma-glutamyl cycle of Saccharomyces cerevisiae and represents a novel family of Cys-Gly peptidases. *The Journal of biological chemistry*, 284(21):14493-14502.

Kelly, P., Stemmle, L.N., Madden, J.F., Fields, T.A., Daaka, Y. & Casey, P.J. 2006. A role for the G12 family of heterotrimeric G proteins in prostate cancer invasion. *The Journal of biological chemistry*, 281(36):26483-26490.

Kelson, T.L., Secor McVoy, J.R. & Rizzo, W.B. 1997. Human liver fatty aldehyde dehydrogenase: microsomal localization, purification, and biochemical characterization. *Biochimica et biophysica acta*, 1335(1-2):99-110.

Kerr, J.F., Wyllie, A.H. & Currie, A.R. 1972. Apoptosis: a basic biological phenomenon with wide-ranging implications in tissue kinetics. *British journal of cancer*, 26(4):239-257.

Khare, P., Singh, V.K. & Bala, L. 2022. Serum deprivation enhanced ethanol-induced toxic responses in A549, lung carcinoma cells. *Journal of Environmental Biology*, 43(1):26-34.

Kikuchi, M., Doi, E., Tsujimoto, I., Horibe, T. & Tsujimoto, Y. 2002. Functional analysis of human P5, a protein disulfide isomerase homologue. *Journal of biochemistry*, 132(3):451-455.

Kluwe, L. 2016. Assessing Specificity of Anticancer Drugs *In Vitro*. *Journal of Visualized Experiments,* (109):53752.

Kosoglou, T., Statkevich, P., Johnson-Levonas, A.O., Paolini, J.F., Bergman, A.J. & Alton, K.B. 2005. Ezetimibe: a review of its metabolism, pharmacokinetics and drug interactions. *Clinical Pharmacokinetics,* 44(5):467-494.

Kramer, W., Girbig, F., Corsiero, D., Pfenninger, A., Frick, W., Jähne, G., Rhein, M., Wendler, W., Lottspeich, F., Hochleitner, E.O., Orsó, E. & Schmitz, G. 2005. Aminopeptidase N (CD13) is a molecular target of the cholesterol absorption inhibitor ezetimibe in the enterocyte brush border membrane. *The Journal of biological chemistry,* 280(2):1306-1320.

Kravtsova-Ivantsiv, Y. & Ciechanover, A. 2012. Non-canonical ubiquitin-based signals for proteasomal degradation. *Journal of Cell Sci*ence, 125(3):539-548.

Kress, M., May, E., Cassingena, R. & May, P. 1979. Simian virus 40-transformed cells express new species of proteins precipitable by anti-simian virus 40 tumor serum. *Journal of Virology,* 31(2):472-483.

Kubbutat, M.H., Jones, S.N. & Vousden, K.H. 1997. Regulation of p53 stability by Mdm2. *Nature,* 387(6630):299-303.

Kuo, Y.C., Shen, Y.R., Chen, H.I., Lin, Y.H., Wang, Y.Y., Chen, Y.R., Wang, C.Y. & Kuo, P.L. 2015. SEPT12 orchestrates the formation of mammalian sperm annulus by organizing core octameric complexes with other SEPT proteins. *Journal of cell science*, 128(5):923-934.

Kussie, P.H., Gorina, S., Marechal, V., Elenbaas, B., Moreau, J., Levine, A.J. & Pavletich, N.P. 1996. Structure of the MDM2 oncoprotein bound to the p53 tumor suppressor transactivation domain. *Science,* 274(5289):948-953.

Lane, D.P. & Crawford, L.V. 1979. T antigen is bound to a host protein in SV40-transformed cells. *Nature*, 278(5701):261-263.

Leach, F.S., Tokino, T., Meltzer, P., Burrell, M., Oliner, J.D., Smith, S., Hill, D.E., Sidransky, D., Kinzler, K.W. & Vogelstein B. 1993. p53 Mutation and MDM2 amplification in human soft tissue sarcomas. *Cancer research,* 53(10):2231-2234.

Lebourgeois, S., Fraisse, A., Hennechart-Collette, C., Guillier, L., Perelle, S. & Martin-Latil, S. 2018. Development of a Real-Time Cell Analysis (RTCA) Method as a Fast and Accurate Method for Detecting Infectious Particles of the Adapted Strain of Hepatitis A Virus. *Frontiers in Cellular Infection Microbiology,* 8:335.

Lee, A.S., Kranzusch, P.J. & Cate, J.H. 2015. eIF3 targets cell-proliferation messenger RNAs for translational activation or repression. *Nature*, 522(7554):111-114.

Lees-Miller, S.P., Sakaguchi, K., Ullrich, S.J., Appella, E. & Anderson, C.W. 1992. Human DNA-activated protein kinase phosphorylates serines 15 and 37 in the amino-terminal transactivation domain of human p53. *Molecular and cellular biology,* 12(11):5041-5049.

Li, L., Deng, B., Xing, G., Teng, Y., Tian, C., Cheng, X., Yin, X., Yang, J., Gao, X., Zhu, Y., Sun, Q., Zhang, L., Xiao, Y & He, F. 2007. PACT is a negative regulator of p53 and essential for cell growth and embryonic development. *Proceedings of the National Academy of Sciences of the United States of America,* 104(19):7951-7956.

Li, M., Brooks, C.L., Wu-Baer, F., Chen, D., Baer, R. & Gu, W. 2003. Mono- versus polyubiquitination: differential control of p53 fate by Mdm2. *Science,* 302(5652):1972-1975.

Li, M., Luo, J., Brooks, C.L. & Gu, W. 2002. Acetylation of p53 inhibits its ubiquitination by Mdm2. *The Journal of biological chemistry,* 277(52):50607-50611.

Linzer, D.I. & Levine, A.J. 1979. Characterization of a 54K dalton cellular SV40 tumor antigen present in SV40-transformed cells and uninfected embryonal carcinoma cells. *Cell*, 17(1):43-52.

Loh, P.G., Yang, H.S., Walsh, M.A., Wang, Q., Wang, X., Cheng, Z., Liu, D. & Song, H. 2009. Structural basis for translational inhibition by the tumour suppressor Pdcd4. *The EMBO journal*, 28(3):274-285.

Lomenick, B., Hao, R., Jonai, N., Chin, R.M., Aghajan, M., Warburton, S., Wang, J., Wu, R.P., Gomez, F., Loo, J.A., Wohlschlegel, J.A., Vondriska, T.M., Pelletier, J., Herschman, H.R., Clardy, J., Clarke, C.F. & Huang, J. 2009. Target identification using drug affinity responsive target stability (DARTS). *Proceedings of the National Academy of Sciences of the United States of America,* 106(51):21984-21989.

Lomenick, B., Jung, G., Wohlschlegel, J.A. & Huang, J. 2011. Target identification using drug affinity responsive target stability (DARTS). *Current Protocols in Chemical Biology*, 3(4):163-180.

Lowe, S.W., Schmitt, E.M., Smith, S.W., Osborne, B.A. & Jacks, T. 1993. p53 is required for radiation-induced apoptosis in mouse thymocytes. *Nature,* 362(6423):847-849.

Ma, A.S., Moran-Jones, K., Shan, J., Munro, T.P., Snee, M.J., Hoek, K.S. & Smith, R. 2002. Heterogeneous nuclear ribonucleoprotein A3, a novel RNA trafficking response element-binding protein. *The Journal of biological chemistry*, 277(20):18010-18020.

Mak, D.W.S., Li, S. & Minchom, A. 2019. Challenging the recalcitrant disease- developing molecularly driven treatments for small cell lung cancer. *European Journal of Cancer,* 119:132-150.

Masutani, M., Sonenberg, N., Yokoyama, S. & Imataka, H. 2007. Reconstitution reveals the functional core of mammalian eIF3. *The EMBO journal*, 26(14):3373-3383.

Mayo, L.D. & Donner, D.B. 2001. A phosphatidylinositol 3-kinase/Akt pathway promotes translocation of Mdm2 from the cytoplasm to the nucleus. *Proceedings of the Natural Academy of Sciences of the United States of America,* 98(20):11598-11603.

Mbita, Z., Meyer, M., Skepu, A., Hosie, M., Rees, J. & Dlamini, Z. 2012. De-regulation of the RBBP6 isoform 3/DWNN in human cancers. *Molecular Cellular Biochemistry,* 362(1-2):249-262.

Meek, D.W. 2015. Regulation of the p53 response and its relationship to cancer. *The Biochemical Journal,* 469(3):325-346.

Meek, D.W. & Anderson, C.W. 2009. Posttranslational modification of p53: cooperative integrators of function. Co*ld Spring Harbor perspectives in biology,* 1(6):a000950.

Mercer, W.E., Shields, M.T., Amin, M., Sauve, G.J., Appella, E., Romano, J.W. & Ullrich, S.J. 1990. Negative growth regulation in a glioblastoma tumor cell line that conditionally expresses human wild-type p53. *Proceedings of the Natural Academy of Sciences of the United States of America*, 87(16):6166-6170.

Momand, J., Zambetti, G.P., Olson, D.C., George D. & Levine, A.J. 1992. The mdm-2 oncogene product forms a complex with the p53 protein and inhibits p53-mediated transactivation. *Cell,* 69(7):1237-1245.

Moll, U.M. & Petrenko, O. 2003. The MDM2-p53 interaction. *Molecular Cancer Research,* 1(14):1001-1008.

Motadi, L.R., Bhoola, K.D. & Dlamini, Z. 2011. Expression and function of retinoblastoma binding protein 6 (RBBP6) in human lung cancer. *Immunobiology*, 216(10):1065-1073.

Motoyama, S., Ladines-Llave, C.A., Villanueva, S.L. & Maruo, T. 2004. The role of human papilloma virus in the molecular biology of cervical carcinogenesis. *The Kobe Journal of Medical Science,* 50(1-2): 9-19.

Murphy, S.A., Cannon, C.P., Blazing, M.A., Giugliano, R.P., White, J.A., Lokhnygina, Y., Reist, C., Im, K., Bohula, E.A., Isaza, D., Lopez-Sendon, J., Dellborg, M., Kher, U., Tershakovec, A.M. & Braunwald, E. 2016. Reduction in Total Cardiovascular Events with Ezetimibe/Simvastatin Post-Acute Coronary Syndrome: The IMPROVE-IT Trial. J*ournal of the American College of Cardiology,* 64(4):353-361.

Nakamura, S., Roth, J.A. & Mukhopadhyay, T. 2000. Multiple lysine mutations in the C-terminal domain of p53 interfere with MDM2-dependent protein degradation and ubiquitination. *Molecular and cellular biology,* 20(24):9391-9398.

Nguyen, S.T., Nguyen, H.T. & Truong, K.D. 2020. Comparative cytotoxic effects of methanol, ethanol and DMSO on human cancer cell lines. *Biomedical Research and Therapy*, 7(7):3855-3859.

Noda, A., Ning, Y., Venable, S.F., Pereira-Smith, O.M. & Smith, J.R. 1994. Cloning of senescent cell-derived inhibitors of DNA synthesis using an expression screen. *Experimental cell research,* 211(1):90-98.

Ogawara, Y., Kishishita, S., Obata, T., Isazawa, Y., Suzuki, T., Tanaka, K., Masuyama, N. & Gotoh, Y. 2002. Akt enhances Mdm2-mediated ubiquitination and degradation of p53. *The Journal of biological chemistry,* 277(24):21843-21850.

Oliner, J.D., Kinzler, K.W., Meltzer, P.S., George, D.L. & Vogelstein, B. 1992. Amplification of a gene encoding a p53-associated protein in human sarcomas. *Nature,* 358(6381):80-83.

Oliner, J.D., Pietenpol, J.A., Thiagalingam, S., Gyuris, J., Kinzler, K.W. & Vogelstein B. 1993. Oncoprotein MDM2 conceals the activation domain of tumour suppressor p53. *Nature,* 362(6423):857-860.

Ong, S.E., Li, X., Schenone, M., Schreiber, S.L. & Carr, S.A. 2012. Identifying cellular targets of small-molecule probes and drugs with biochemical enrichment and SILAC. *Methods in molecular biology*, 803:129-140.

Oren, M. 2003. Decision making by p53: life, death and cancer. *Cell Death and Differentiation,* 30(4):431-442.

Pai, M.Y., Lomenick, B., Hwang, H., Schiestl, R., McBride, W., Loo, J.A. & Huang, J. 2015. Drug affinity responsive target stability (DARTS) for small-molecule target identification. *Methods in molecular biology (Clifton, N.J.)*, *1263*:287-298.

Patil, S.P., Ballester, P.J. & Kerezsi, C.R. 2014. Prospective virtual screening for novel p53–MDM2 inhibitors using ultrafast shape recognition. *Journal of Computer-Aided Molecular Design,* 28(2):89-97.

Peattie, D.A., Harding, M.W., Fleming, M.A., DeCenzo, M.T., Lippke, J.A., Livingston, D.J. & Benasutti, M. 1992. Expression and characterization of human FKBP52, an immunophilin that associates with the 90-kDa heat shock protein and is a component of steroid receptor complexes. *Proceedings of the National Academy of Sciences of the United States of America*, 89(22):10974-10978.

Phan, B.A.P., Dayspring, T.D. & Toth, P.P. 2012. Ezetimibe therapy: mechanism of action and clinical update. *Vascular Health and Risk Management,* 8(1):415-427.

Pickart, C.M. 2001. Mechanisms underlying ubiquitination. *Annual Review of Biochem*istry, 70:503-533.

Politi, K. & Herbst, R. S. 2015. Lung cancer in the era of precision medicine. *Clinical Cancer Research,* 21:2213-2220.

Polyak, K., Waldman, T., He, T.C., Kinzler, K.W. & Vogelstein, B. 1996. Genetic determinants of p53-induced apoptosis and growth arrest. *Genes & development,* 10(15):1945-1952.

Pugh, D.J.R., AB, E., Faro, A., Lutya, P.T., Hoffmann, E. & Rees, D.J.G. 2006. DWNN, a novel ubiquitin-like domain, implicates RBBP6 in mRNA processing and ubiquitin-like pathways. *BMC Structural Biology,* 6(1):3-8.

Rauch, J.N. & Gestwicki, J.E. 2014. Binding of Human Nucleotide Exchange Factors to Heat Shock Protein 70 (Hsp70) Generates Functionally Distinct Complexes *in Vitro*. *Protein Synthesis and Degradation*, 289(3):1402-1414.

Robinson, T.J., Pai, M., Liu, J.C., Vizeacoumar, F., Sun, T., Egan, S.E., Datti, A., Huang, J. & Zacksenhaus, E. 2013. High-throughput screen identifies disulfiram as a potential therapeutic for triple-negative breast cancer cells: interaction with IQ motif-containing factors. *Cell cycle (Georgetown, Tex.)*, *12*(18), 3013-3024.

Rodriguez, M.S., Desterro, J.M., Lain, S., Lane, D.P. & Hay, R.T. 2000. Multiple C-terminal lysine residues target p53 for ubiquitin-proteasome-mediated degradation. *Molecular and cellular biology,* 20(22):8458-8467.

Rosenblum, S.B., Huynh, T., Afonso, A., Davis, H.R. Jr., Yumibe, N., Clader, J.W. & Burnett, D.A. 1998. Discovery of 1-(4-fluorophenyl)-(3R)-[3-(4-fluorophenyl)-(3S)-hydroxypropyl]-(4S)-(4 -hydroxyphenyl)-2-azetidinone (SCH 58235): a designed, potent, orally active inhibitor of cholesterol absorption. *Journal of Medicinal Chemistry,* 41(6):973-980.

Roth, J., Dobbelstein, M., Freedman, D.A., Shenk, T. & Levine, A.J. 1998. Nucleo-cytoplasmic shuttling of the hdm2 oncoprotein regulates the levels of the p53 protein via a pathway used by the human immunodeficiency virus rev protein. *The EMBO Journal,* 17(2):554-564.

Ryan, J.J., Prochownik, E., Gottlieb, C.A., Apel, I.J., Merino, R., Nunez, G. & Clarke, M.F. 1994. *c-myc* and *bcl-2* modulate p53 function by altering p53 subcellular trafficking during the cell cycle. *Proceedings of the Natural Academy of Science of the United States of America*, 91(13):5878-5882.

Saijo, M., Sakai, Y., Kishino, T., Niikawa, N., Matsuura, Y., Morino, K., Tamai, K. & Taya, Y. 1995. Molecular cloning of a human protein that binds to the retinoblastoma protein and chromosomal mapping. *Genomics*, 27(3):511-519.

Saito, S., Goodarzi, A.A., Higashimoto, Y., Noda, Y., Lees-Miller, S.P., Appella, E. & Anderson, C.W. 2002. ATM mediates phosphorylation at multiple p53 sites, including Ser(46), in response to ionizing radiation. *The Journal of biological chemistry,* 277(15):12491-12494.

Saji, S., Nakashima, S., Hayashi, S., Toi, M., Saji, S. & Nozawa, Y. 1999. Overexpression of MDM2 in MCF-7 promotes both growth advantage and p53 accumulation in response to estradiol. *Japanese journal of cancer research: Gann*, 90(2):210-218.

Sakaguchi, K., Saito, S., Higashimoto, Y., Roy, S., Anderson, C.W. & Appella, E. 2000. Damage-mediated phosphorylation of human p53 threonine 18 through a cascade mediated by a casein 1-like kinase. Effect on Mdm2 binding. *The Journal of biological chemistry,* 275(13):9278-9283.

Sanchez, E.R., Faber, L.E., Henzel, W.J. & Pratt, W.B. 1990. The 56-59-kilodalton protein identified in untransformed steroid receptor complexes is a unique protein that exists in cytosol in a complex with both the 70- and 90-kilodalton heat shock proteins. *Biochemistry*, 29(21):5145-5152.

Sanders, R.J., Ofman, R., Dacremont, G., Wanders, R.J. & Kemp, S. 2008. Characterization of the human omega-oxidation pathway for omega-hydroxy-very-long-chain fatty acids. *FASEB journal : official publication of the Federation of American Societies for Experimental Biology*, 22(6):2064-2071.

Schägger, H. 2006. Tricine-SDS-PAGE. *Nature Protocols*, 1:16-22.

Selvakumaran, M., Lin, H.K., Miyashita, T., Wang, H.G., Krajewski, S., Reed, J.C., Hoffman, B. & Liebermann, D. 1994. Immediate early up-regulation of *bax* expression by p53 but not TGF beta 1: a paradigm for distinct apoptotic pathways. *Oncogene,* 9(6):1791-1798.

Sherr, C.J. & McCormick, F. 2002. The RB and p53 pathways in cancer. *Cancer Cell,* 2(2):103-112.

Shevchenko, A., Tomas, H., Havli, J., Olsen, J.V. & Mann, M. 2006. In-gel digestion for mass spectrometric characterization of proteins and proteomes. *Nature Protocols,* 1(6):2856-2860.

Shieh, S.Y., Ahnm J., Tamaim K., Tayam Y. & Prives, C. 2000. The human homologs of checkpoint kinases Chk1 and Cds1 (Chk2) phosphorylate p53 at multiple DNA damage-inducible sites. *Genes & development,* 14(3):289-300.

Shieh, S.Y., Ikeda, M., Taya, Y. & Prives, C. 1997. DNA damage-induced phosphorylation of p53 alleviates inhibition by MDM2. *Cell,* 91(3):325-334.

Shiloh, Y. 2001. ATM and ATR: networking cellular responses to DNA damage. *Current Opinion in Genetics Development,* 11(1):71-77.

Siliciano, J.D., Canman, C.E., Taya, Y., Sakaguchi, K., Appella, E. & Kastan, M.B. 1997. DNA damage induces phosphorylation of the amino terminus of p53. *Genes & development,* 11(24):3471-3481.

Simons, A., Melamed-Bessudo, C., Wolkowicz, R., Sperling, J., Sperling, R., Eisenbach, L. & Rotter, V. 1997. PACT: cloning and characterization of a cellular p53 binding protein that interacts with Rb. *Oncogene*,14(2):145-155.

Sluss, H.K., Armata, H., Gallant, J. & Jones, S.N. 2004. Phosphorylation of serine 18 regulates distinct p53 functions in mice. *Molecular and cellular biology,* 24(3):976-984.

Sozzi, G., Miozzo, M., Pastorino, U., Pilotti, S., Donghi, R., Giarola, M., De Gregorio, L., Manenti, G., Radice, P., & Minoletti, F. 1995. Genetic evidence for an independent origin of multiple preneoplastic and neoplastic lung lesions. *Cancer research*, 55(1):135-140.

Stark, J.L., Mehla, K., Chaika, N., Acton, T.B., Xiao, R., Singh, P.K., Montelione, G.T. & Powers, R. 2014. Structure and function of human DnaJ homologue subfamily a member 1 (DNAJA1) and its relationship to pancreatic cancer. *Biochemistry*, 53(8):1360-1372.

Sugahara, T., Nakajima, H., Shirahata, S. & Murakami, H. 1992. Purification and characterization of immunoglobulin production stimulating factor-II beta derived from Namalwa cells. *Cytotechnology*, 10(2):137-146.

Sun, W., Tanaka, T.Q., Magle, C.T., Huang, W., Southall, N., Huang, R., Dehdashti, S.J., McKew, J. C., Williamson, K.C. & Zheng, W. 2014. Chemical signatures and new drug targets for gametocytocidal drug development. *Scientific reports*, 4:3743.

Sung, H., Ferlay, J., Siegel, R. L., Laversanne, M., Soerjomataram, I., Jemal, A. & Bray, F. 2021. Global cancer statistics 2020: GLOBOCAN estimates of incidence and mortality worldwide for 36 cancers in 185 countries. *CA: A Cancer Journal for Clinicians*, 71(3):209-249.

Tatham, M.H., Jaffray, E., Vaughan, O.A., Desterro, J.M., Botting, C.H., Naismith, J.H. & Hay, R.T. 2001. Polymeric chains of SUMO-2 and SUMO-3 are conjugated to protein substrates by SAE1/SAE2 and Ubc9. *The Journal of biological chemistry*, 276(38):35368-35374.

Temel, R.E., Tang, W., Ma, Y., Rudel, L.L., Willingham, M.C., Loannou, Y.A., Davies, J.P., Nilsson, L. & Yu, L. 2007. Hepatic Niemann-Pick C1-like 1 regulates biliary cholesterol concentration and is a target of ezetimibe. *The Journal of Clinical Investigation,* 117(7):1968-1978.

Teufel, M., Saudek, V., Ledig, J.P., Bernhardt, A., Boularand, S., Carreau, A., Cairns, N.J., Carter, C., Cowley, D.J., Duverger, D., Ganzhorn, A.J., Guenet, C., Heintzelmann, B., Laucher, V., Sauvage, C. & Smirnova, T. 2003. Sequence identification and characterization of human carnosinase and a closely related non-specific dipeptidase. *The Journal of biological chemistry*, 278(8):6521-6531.

Tohda, C., Urano, T., Umezaki, M., Nemere, I. & Kuboyama, T. 2012. Diosgenin is an exogenous activator of 1,25D_3-MARRS/Pdia3/ERp57 and improves Alzheimer's disease pathologies in 5XFAD mice. *Scientific reports*, 2:535.

Twala, C.S. 2017. Drugs targeting the retinoblastoma binding protein 6 (RBBP6). Johannesburg: Wits. (Dissertation - MSc).

Ubanako, P.N. 2015. Targeting retinoblastoma binding protein 6 (RBBP6) as an anti-ovarian cancer therapeutic strategy. Johannesburg: Wits. (Dissertation - MSc).

Unger, T., Juven-Gershon, T., Moallem, E., Berger, M., Vogt Sionov, R., Lozano, G., Oren, M. & Haupt, Y. 1999. Critical role for Ser20 of human p53 in the negative regulation of p53 by Mdm2. *The EMBO Journal,* 18(7):1805-1814.

van Karnebeek, C.D.M., Ramos, R.J., Wen, X.Y., Tarailo-Graovac, M., Gleeson, J.G., Skrypnyk, C., Brand-Arzamendi, K., Karbassi, F., Issa, M.Y., van der Lee, R., Drögemöller, B.I., Koster, J., Rousseau, J., Campeau, P.M., Wang, Y., Cao, F., Li, M., Ruiter, J., Ciapaite, J., Kluijtmans, L.A.J. & Wevers, R. A. 2019. Bi-allelic GOT2 Mutations Cause a Treatable Malate-Aspartate Shuttle-Related Encephalopathy. *American journal of human genetics*, 105(3):534-548.

Ventura, A., Kirsch, D.G., McLaughlin, M.E., Tuveson, D.A., Grimm, J., Lintault, L., Newman, J., Reczek, E.E., Weissleder, R. & Jacks, T. 2007. Restoration of p53 function leads to tumour regression in vivo. *Nature*, 445(7128):661-665.

Vogelstein, B. & Kinzler, K.W. 1992. P53 function and dysfunction. *Cell,* 70(4):523-526.

Vousden, K.H. & Lu, X. Live or let die: the cell's response to p53. *Nature Reviews. Cancer,* 2(8):594-604.

Vousden, K.H. & Prives, C. 2009. Blinded by the Light: The Growing Complexity of p53. *Cell,* 137(3):413-431.

Wang, Y., Blandino, G. & Givol, D. 1999. Induced p21waf expression in H1299 cell line promotes cell senescence and protects against cytotoxic effect of radiation and doxorubicin. *Oncogene,* 18(16):2643-2649.

Wang, Y., Szekely, L., Okan, I., Klein, G. & Wiman, K.G. 1993. Wild-type p53-triggered apoptosis is inhibited by *bcl-2* in a *v-myc*-induced T-cell lymphoma line. *Oncogene,* 8(12):3427-3431.

White, M.K. & Cinti, C. 2004. A morphologic approach to detect apoptosis based on electron microscopy. *Methods in molecular biology (Clifton, N.J.)*, 285:105-111.

Witte, M.M. & Scott, R.E. 1997. The proliferation potential protein-related (P2P-R) gene with domains encoding heterogeneous nuclear ribonucleoprotein association and Rb1 binding shows repressed expression during terminal differentiation. *Proceedings of the National Academy of Sciences of the United States of America,* 94(4):1212-1217.

Wood, M.A., McMahon, S.B. & Cole, M.D. 2000. An ATPase/helicase complex is an essential cofactor for oncogenic transformation by c-Myc. *Molecular cell*, 5(2):321-330.

Wu, L. & Levine, A.J. 1997. Differential regulation of the p21/WAF-1 and mdm2 genes after high-dose UV irradiation: p53-dependent and p53-independent regulation of the mdm2 gene. *Molecular Medicine,* 3(7):441-451.

Xue, W., Zender, L., Miething, C., Dickins, R.A., Hernando, E., Krizhanovsky, V., Cordon-Cardo, C. & Lowe, S.W. 2007. Senescence and tumour clearance is triggered by p53 restoration in murine liver carcinomas. *Nature*, 445(7128):656-660.

Yoshitake, Y., Nakatsura, T., Monji, M., Senju, S., Matsuyoshi, H., Tsukamoto, H., Hosaka, S., Komori, H., Fukuma, D., Ikuta, Y., Katagiri, T., Furukawa, Y., Ito, H., Shinohara, M., Nakamura, Y. & Nishimura, Y. 2004. Proliferation potential-related protein, an ideal oesophageal cancer antigen for immunotherapy, identified using complementary DNA microarray analysis. *Clinical Cancer Research,*10(19):6437-6448.

Zhang, B., Zhang, T., Wang, G., Wang, G., Chi, W., Jiang, Q. & Zhang, C. 2015. GSK3β-Dzip1-Rab8 cascade regulates ciliogenesis after mitosis. *PLoS biology*, 13(4):e1002129.

Zhang, P., Chan, D.W., Zhu, Y., Li, J.J., Ng, I.O., Wan, D. & Gu, J. 2006. Identification of carboxypeptidase of glutamate like-B as a candidate suppressor in cell growth and metastasis in human hepatocellular carcinoma. *Clinical cancer research : an official journal of the American Association for Cancer Research*, 12(22):6617-6625.

Zhang, Z., Miao, L., Xin, X., Zhang, J., Yang, S., Miao, M., Kong, X. & Jiao, B. 2014. Underexpressed CNDP2 participates in gastric cancer growth inhibition through activating the MAPK signaling pathway. *Molecular medicine (Cambridge, Mass.)*, 20(1):17-28.

Zhou, B.P., Liao, Y., Xia, W., Zou, Y., Sponhn, B. & Hung, M.C. 2001. HER-2/neu induces p53 ubiquitination via Akt-mediated MDM2 phosphorylation. *Nature Cell Biology,* 3(11):973-982.

Zhou, P., Yao, Y., Soh, J.W. & Weinstein, I.B. 1999. Overexpression of p21Cip1 or p27Kip1 in the promyelocytic leukemia cell line HL60 accelerates its lineage-specific differentiation. *Anticancer Research*, 19(6B):4935-4945.

Zhou, S.L., Gordon, R.E., Bradbury, M., Stump, D., Kiang, C.L. & Berk, P.D. 1998. Ethanol up-regulates fatty acid uptake and plasma membrane expression and export of mitochondrial aspartate aminotransferase in HepG2 cells. *Hepatology (Baltimore, Md.)*, 27(4):1064-1074.

Ziegler, S., Pries, V., Hedberg, C. & Waldmann, H. 2013. Target identification for small bioactive molecules: finding the needle in the haystack. *Angewandte Chemie (International ed. in English)*, 52(10):2744-2792.

Zilfou, J.T. & Lowe, S.W. 2009. Tumor suppressive functions of p53. *Cold Spring Harbor Perspective Biology,* 1(5):a001883.

Zitting, A., Husgafvel-Pursianen, K. & Rantanen, J. 2002. Environmental tobacco smoke – a major preventable cause of impaired health at work. *Scandinavian Journal of Work, Environment and Health,* 28(2):3-6.

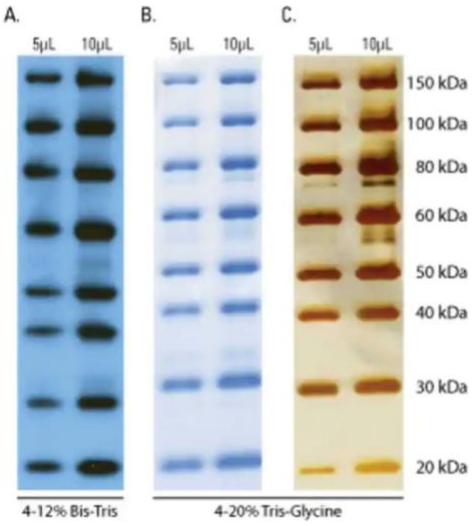

Figure A 1: **SuperSignal™ Enhanced Molecular Weight Protein Ladder**

A

Tube: Tube_001_A549_Untreated

Population	#Events	%Parent	%Total
All Events	20,000	####	100.0
Q1	0	0.0	0.0
Q2	38	0.2	0.2
Q3	19,845	99.2	99.2
Q4	117	0.6	0.6

Tube: Tube_002_A549_Untreated

Population	#Events	%Parent	%Total
All Events	20,000	####	100.0
Q1	3	0.0	0.0
Q2	263	1.3	1.3
Q3	17,594	88.0	88.0
Q4	2,140	10.7	10.7

Tube: Tube_003_A549_Untreated

Population	#Events	%Parent	%Total
All Events	20,000	####	100.0
Q1	1	0.0	0.0
Q2	223	1.1	1.1
Q3	18,088	90.4	90.4
Q4	1,688	8.4	8.4

B

Tube: Tube_001_A549_Vehicle

Population	#Events	%Parent	%Total
All Events	30,000	####	100.0
Q1	3	0.0	0.0
Q2	266	0.9	0.9
Q3	28,167	93.9	93.9
Q4	1,564	5.2	5.2

Tube: Tube_002_A549_Vehicle

Population	#Events	%Parent	%Total
All Events	20,000	####	100.0
Q1	1	0.0	0.0
Q2	213	1.1	1.1
Q3	16,750	83.8	83.8
Q4	3,036	15.2	15.2

Tube: Tube_003_A549_Vehicle

Population	#Events	%Parent	%Total
All Events	20,000	####	100.0
Q1	3	0.0	0.0
Q2	250	1.2	1.2
Q3	17,594	88.0	88.0
Q4	2,153	10.8	10.8

C

Tube: Tube_001_A549_20uM_Eze

Population	#Events	%Parent	%Total
All Events	20,000	####	100.0
Q1	1	0.0	0.0
Q2	542	2.7	2.7
Q3	17,052	85.3	85.3
Q4	2,405	12.0	12.0

Tube: Tube_002_A549_20uM_Eze

Population	#Events	%Parent	%Total
All Events	30,000	####	100.0
Q1	7	0.0	0.0
Q2	666	2.2	2.2
Q3	25,249	84.2	84.2
Q4	4,078	13.6	13.6

Tube: Tube_003_A549_20uM_Eze

Population	#Events	%Parent	%Total
All Events	30,000	####	100.0
Q1	3	0.0	0.0
Q2	455	1.5	1.5
Q3	26,802	89.3	89.3
Q4	2,740	9.1	9.1

D

Tube: Tube_001_A549_40uM_Eze

Population	#Events	%Parent	%Total
All Events	30,000	####	100.0
Q1	4	0.0	0.0
Q2	521	1.7	1.7
Q3	26,872	89.6	89.6
Q4	2,603	8.7	8.7

Tube: Tube_002_A549_40uM_Eze

Population	#Events	%Parent	%Total
All Events	30,000	####	100.0
Q1	2	0.0	0.0
Q2	444	1.5	1.5
Q3	27,197	90.7	90.7
Q4	2,357	7.9	7.9

Tube: Tube_003_A549_40uM_Eze

Population	#Events	%Parent	%Total
All Events	30,000	####	100.0
Q1	2	0.0	0.0
Q2	395	1.3	1.3
Q3	27,228	90.8	90.8
Q4	2,375	7.9	7.9

E

Tube: Tube_001_A549_60uM_Eze

Population	#Events	%Parent	%Total
All Events	20,000	####	100.0
Q1	1	0.0	0.0
Q2	255	1.3	1.3
Q3	19,195	96.0	96.0
Q4	549	2.7	2.7

Tube: Tube_002_A549_60uM_Eze

Population	#Events	%Parent	%Total
All Events	50,000	####	100.0
Q1	3	0.0	0.0
Q2	410	0.8	0.8
Q3	48,347	96.7	96.7
Q4	1,240	2.5	2.5

Tube: Tube_003_A549_60uM_Eze

Population	#Events	%Parent	%Total
All Events	50,000	####	100.0
Q1	1	0.0	0.0
Q2	625	1.2	1.2
Q3	45,721	91.4	91.4
Q4	3,653	7.3	7.3

Figure A 2: **Statistical data of A549 treated with ezetimibe in stages of apoptosis.** The statistical data of A549 cells treated with ezetimibe in the different stages of apoptosis is shown. **A**: untreated samples; **B**: ethanol vehicle; **C**: 20 µM ezetimibe; **D**: 40 µM ezetimibe; **E**: 60 µM ezetimibe.

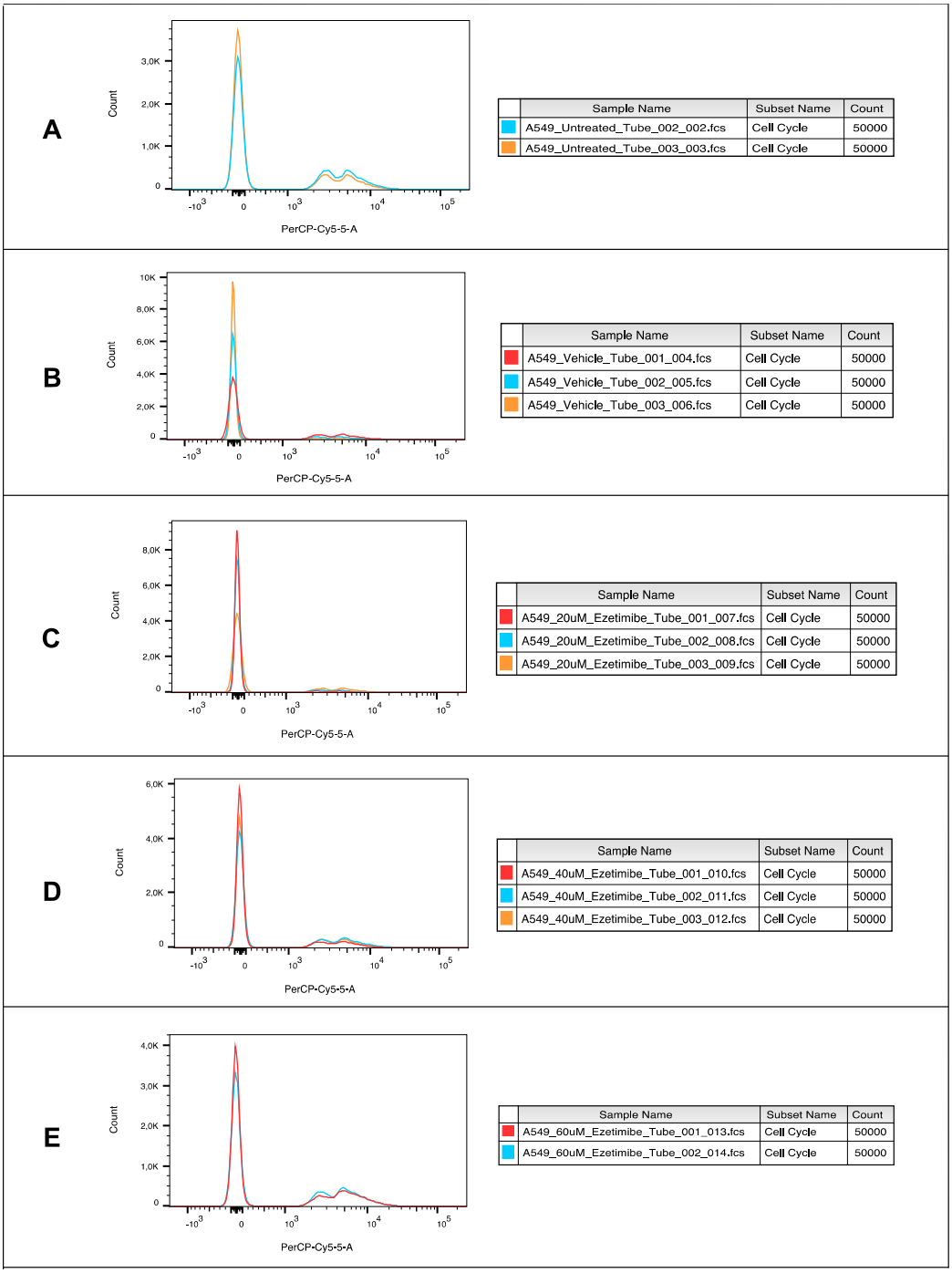

Figure A 3: Overlayed results of A549 cell cycle analysis. The histograms seen in figure 3.5 are overlayed per drug treatment. **A**: untreated; **B**: ethanol vehicle; **C**: 20 µM ezetimibe; **D**: 40 µM ezetimibe; **E**: 60 µM ezetimibe.

Table A 1: **Statistical data of flow cytometry cell cycle analysis**

		Cell Population %				
		G1 Phase	S Phase	G2 Phase	< G1	> G2
Tube 1	Untreated	n/a	n/a	n/a	n/a	n/a
Tube 2	Untreated	62	-30	70	2	5

Tube 3	**Untreated**	71	-5	34	2	0
Tube 1	**Ethanol Vehicle**	71	-3	32	0	1
Tube 2	**Ethanol Vehicle**	82	-1	20	0	0
Tube 3	**Ethanol Vehicle**	93	0	6	0	0
Tube 1	**20 µM Ezetimibe**	91	-3	10	0	0
Tube 2	**20 µM Ezetimibe**	86	0	14	0	0
Tube 3	**20 µM Ezetimibe**	78	-2	23	0	0
Tube 1	**40 µM Ezetimibe**	77	-6	28	0	0
Tube 2	**40 µM Ezetimibe**	69	-5	36	0	1
Tube 3	**40 µM Ezetimibe**	73	-3	30	0	0
Tube 1	**60 µM Ezetimibe**	64	-7	43	0	2
Tube 2	**60 µM Ezetimibe**	60	-27	71	2	5
Tube 3	**60 µM Ezetimibe**	n/a	n/a	n/a	n/a	n/a

Table A 2: **Cell line information**

	Cell Cultures		
	HEK293	**A549**	**MCF-7**
Host	Human	Human	Human
Diagnosis	Normal	Lung Cancer	Breast Cancer
p53 Status	Wild Type	Wild Type	Wild Type
Supplier	Dr Jitcy Saji Joseph	Separation Scientific, SA	Dr Jitcy Saji Joseph

Table A 3: Cell culture reagents

Reagent	**Supplier and Catalog Number**
Dulbecco's modified eagle medium	Biowest (L0104)
Fetal bovine serum	Biowest (S1300)
L-Glutamine	Biowest (X0550)
Penicillin-streptomycin	Biowest (L0018)
Phosphate-buffered saline	Biowest (X0520)
Trypsin-EDTA	Biowest (X0930)

Table A 4: Reagents and chemicals

Name	**Supplier and Catalog Number**
Acetic acid	Sigma-Aldrich (71251)
Acrylamide/Bis-acrylamide (30%)	Sigma-Aldrich (A3699)
Ammonium Persulfate (APS)	Sigma-Aldrich (A3678)

β-Mercaptoethanol	Thermo Fisher Scientific (31350010)
Calcium Chloride	Sigma-Aldrich (C4901)
Coomassie Brilliant Blue	Bio-Rad (1610786)
Dimethyl sulfoxide	Sigma-Aldrich (276855)
Ethyl alcohol	Sigma-Aldrich (E7023)
Ezetimibe	Sigma-Aldrich (SML1629)
Glycerol	Sigma-Aldrich (G5516)
Hydrogen Chloride	Sigma-Aldrich (295426)
Methyl alcohol	UPS (1424109)
MTT solution	ScienCell Research Laboratories (8028)
Sodium Chloride	Sigma-Aldrich (S5886)
Sodium dodecyl sulfate	Sigma-Aldrich (L3771)
Sodium Fluoride	Sigma-Aldrich (S6776)
Tetramethylethylenediamine (TEMED)	Thermo Fisher Scientific (17919)
Tricine	Sigma-Aldrich (T0377)
Tris(hydroxymethyl)aminomethane	Sigma-Aldrich (252859)
Tris hydrochloride	Roche (10812846001)
Triton-X 100	Thermo Fisher Scientific (HFH10)

Table A 5: Laboratory kits

Name	Supplier and Catalog Number
Annexin V-FITC Apoptosis Detection Kit	Sigma-Aldrich (A9210)
Propidium Iodide (1mg/mL)	Invitrogen (P3566)
Pronase (10 mg/ml)	Sigma-Aldrich (11 459 643 001)
RNase (110 000 U/mL)	abcam (ab139418)
SuperSignal™ Enhanced Molecular Weight Protein Ladder	Thermo Fisher Scientific (84786)

Table A 6: Solution buffers composition

Buffer	Composition
Recovery media	20% FBS, 1 % penicillin-streptomycin, 79% DMEM media, 1% L-Glutamine
Maintenance media	10% FBS, 1% penicillin-streptomycin, 89% DMEM media, 1% L-Glutamine
Freezing media	10% DMSO, 90% FBS
5 x Annexin-binding buffer	50 mM HEPES, 700 mM NaCl, 12.5 mM $CaCl_2$ (pH 7.4)
1 x Annexin-binding buffer	One part 5 x Annexin-binding buffer, four parts ddH_2O
PI working solution (100 µg/mL)	5 µL 1mg/mL PI stock solution diluted in 45 µL 1 x Annexin-binding buffer
PI + RNase Staining solution	9.45 mL PBS, 500 µL 20x PI (1mg/mL), 50 µL 200x RNaseA (110.000U/mL)
Lysis buffer	958 µL 2 x Triton-X Lysis buffer, 2 µL 1 M NaF solution, 40 µL Protease Inhibitor solution
2 x Triton-X Lysis buffer	0,4% Triton-X 100, 400 mM NaCl, 100 mM Tris-HCl (pH 7.5), 20% glycerol
10 x TNC buffer	500 mM Tris-HCl with pH 8.0, 500 mM NaCl, 100 mM $CaCl_2$

1 x TNC buffer	10 µL 10 x TNC buffer, 90 µL ddH_2O
Sample buffer	12% SDS, 6% β-Mercaptoethanol, 30% glycerol, 0.05% Coomassie Brilliant Blue, 150 mM Tris-HCl with pH 7.0
Coomassie Blue stain	250 mL of 50% methanol, 0.25g Coomassie Brilliant Blue, 50 mL acetic acid, 200 mL ddH_2O
SDS-PAGE destain	50 mL ethanol, 70 mL acetic acid, 880 mL ddH_2O

Table A 7: Laboratory equipment

Equipment	Supplier
Neubauer-improved Counting Chamber	Marienfeld Superior (REF0610010)
Varioskan Flash Microplate Reader	Thermo Fisher
BD FACSAria™ III Cell Sorter	BD Biosciences
Vertical Electrophoresis Chamber and Power Supply	Bio-Rad
GelDoc Imaging System	Bio-Rad

Table A 8: Statistical analysis - Mean ± SD

	MTT Assay		
Concentration	**HEK293**	**A549**	**MCF-7**
0 µM Ezetimibe	100.0 ± 0.0	100.0 ± 0.0	100.0 ± 0.0
10 µM Ezetimibe	107.6 ± 10.8	94.8 ± 20.2	99.7 ± 11.6
20 µM Ezetimibe	121.0 ± 13.5	81.1 ± 8.4	103.1 ± 32.1
30 µM Ezetimibe	135.2 ± 2.3	52.1 ± 19.7	88.7 ± 24.8
40 µM Ezetimibe	120.1 ± 27.0	41.8 ± 15.2	124.7 ± 37.3
60 µM Ezetimibe	131.8 ± 49.1	39.9 ± 20.3	111.0 ± 28.9
80 µM Ezetimibe	121.7 ± 47.1	53.7 ± 38.9	107.9 ± 20.9
	Apoptosis		
Concentration	**Live Cells**	**Early-Stage Apoptosis**	**Late-Stage Apoptosis**
0 µM Ezetimibe	92.8 ± 5.6	6.3 ± 5.0	0.9 ± 0.6
60 µM Ethanol Vehicle	88.6 ± 5.1	10.4 ± 5.0	1.1 ± 0.2
20 µM Ezetimibe	86.3 ± 2.7	11.6 ± 2.3	2.1 ± 0.6
40 µM Ezetimibe	90.4 ± 0.7	8.2 ± 0.5	1.5 ± 0.2
60 µM Ezetimibe	94.7 ± 2.879	4.2 ± 2.7	1.1 ± 0.3
	Cell cycle analysis		
Concentration	**G2 Phase**	**S Phase**	**G1 Phase**
0 µM Ezetimibe	52.0 ± 25.5	-17.5 ± 17.7	66.5 ± 6.4
60 µM Ethanol Vehicle	19.3 ± 13.0	-1.3 ± 1.5	82.0 ± 11.0
20 µM Ezetimibe	15.7 ± 6.7	-1.7 ± 1.5	85.0 ± 6.6
40 µM Ezetimibe	31.3 ± 4.2	-4.7 ± 1.5	73.0 ± 4.0
60 µM Ezetimibe	57.0 ± 19.8	-17.0 ± 14.1	62.0 ± 2.8

Table A 9: Statistical analysis - Statistical significance

	MTT Assay	
Concentration	**HEK293 vs MCF-7**	**HEK293 vs A549**
0 µM Ezetimibe	> 0.9999	> 0.9999
10 µM Ezetimibe	0.9905	0.7712
20 µM Ezetimibe	0.6183	0.0071
30 µM Ezetimibe	0.0083	< 0.0001
40 µM Ezetimibe	0.9997	< 0.0001
60 µM Ezetimibe	0.4567	< 0.0001
80 µM Ezetimibe	0.8568	< 0.0001

	Apoptosis		
Concentration	**Live cells**	**Early-Stage Apoptosis**	**Late-Stage Apoptosis**
60 µM Ethanol Vehicle	0.5663	0.6086	> 0.9999
20 µM Ezetimibe	0.1842	0.3752	0.9906
40 µM Ezetimibe	0.9010	0.9637	0.9994
60 µM Ezetimibe	0.9613	0.9354	> 0.9999

	Cell cycle analysis		
Concentration	**G2 Phase**	**S Phase**	**G1 Phase**
60 µM Ethanol Vehicle	0.0128	0.4200	0.4613
20 µM Ezetimibe	0.0049	0.4405	0.2910
40 µM Ezetimibe	0.1972	0.6365	0.9530
60 µM Ezetimibe	0.9870	> 0.9999	0.9912